Stress-displacement stabilized finite element analysis of thin structures using solid-shell elements—Part I: On the need of interpolating the stresses

A. Aguirre[a,b], R. Codina[a,c], J. Baiges[a,c]
[a] Universitat Politècnica de Catalunya, Jordi Girona 1 − 3, Edifici C1, Barcelona 08034, Spain.
[b] Universidad de Santiago de Chile, Av. Libertador Bernardo O'Higgins 3363, Estación Central, Santiago, Chile.
[c] Centre Internacional de Mètodes Numèrics en Enginyeria (CIMNE), Gran Capità s/n, Edifici C1, Barcelona 08034, Spain.
alejandro.aguirre@upc.edu (A. Aguirre), ramon.codina@upc.edu (R. Codina), joan.baiges@upc.edu (J. Baiges)

Abstract

This work studies the solid-shell finite element approach to approximate thin structures using a stabilized mixed displacement-stress formulation based on the Variational Multiscale framework. The work is divided in two parts. In Part I, the numerical locking effects inherent to the solid-shell approach are characterized using a variety of benchmark problems in the infinitesimal strain approximation. In Part II, the results are extended to formulate the mixed approach in finite strain hyperelastic problems. In the present work, the stabilized mixed displacement-stress formulation is proven to be adequate to deal with all kinds of numerical locking. Additionally, a more comprehensive analysis of each individual type of numerical locking, how it is triggered and how it is overcome is also provided. The numerical locking usually occurs when parasitic strains overtake the system of equations through specific components of the stress tensor. To properly analyze them, the direction of each component of the stress tensor has been defined respect to the shell directors. Therefore, it becomes necessary to formulate the solid-shell problem in curvilinear coordinates, allowing to give mechanical meaning to the stress components (shear, twisting, membrane and thickness stresses) independently of the global frame of reference. The conditions in which numerical locking is triggered as well as the stress tensor component responsible of correcting the locking behavior have been identified individually by characterizing the numerical response of a set of different benchmark problems.

Keywords: `Mixed Formulation, Solid-Shell, Stabilization, Numerical locking`

1. Introduction

Structural elements have played an important role in the development of technology. The reason is that thin structures are the most common in nature and have proven to be essential engineering tools along history [1]. They are usually modeled as a dimensional reduction of a 3D solid where one or two of its dimensions are much thinner than the others. In this manner, beam and rod formulations have been developed to approximate thin structures with two reduced dimensions, while plate and shell formulations have been developed to model structures of a single dimension reduction [2].

In the finite element literature, shell models are usually classified into three different groups: the classical shell elements, the continuum based elements and the solid-shell elements. As the name suggest, the classical shell elements are based on conventional theories of plates and shells [3, 4, 5, 6, 7, 8, 9, 10, 11]; therefore, they inherently use rotational degrees of freedom to describe the kinematics with respect to the mid-surface of the shell. The continuum based shell elements, usually called degenerated elements, were first introduced by Ahmad et al. [12]. These elements are directly constructed from the continuum equations [13, 14, 15]. The derivation of these elements is straightforward, and it requires to enforce kinematic constrains to the upper and lower surfaces with respect to the shell mid-surface using rotational degrees of freedom, and thus, the enforcement of the inextensibility of the shell director. Both classical and continuum based approaches usually require to either impose the inextensibility of the director or to enforce the plane stress constraint [16, 13]; the reader can also refer to [17, 18] for a comparison between these two approaches. The solid-shell approach consists in the approximation of thin structures using 3D elements; the idea was first introduced by Hauptmann et al. [19]. In other words, this approach employs a 3D solid approximation that explicitly considers the nodes at the upper and lower surfaces of the structure and uses displacement degrees of freedom. This approach takes the advantage of not requiring additional kinematic

assumptions and allows the use of three dimensional constitutive equations, at the cost of an increased size of the system of equations.

The most important difference between the approaches described comes from the treatment of the through-the-thickness integration. In regard of this, Bischoff et al. [20] made a comprehensive revision concerning the models used for finite element approximations of thin structures. This reference revises in depth the three approaches, in the linear and non-linear cases. What all approaches share in common is the tendency to suffer numerical locking. In this context, classical shell elements are subject to shear and membrane locking. However, continuum based shell and solid-shell elements are also subject to trapezoidal and thickness locking, particularly using low order elements [21].

The present work focuses specifically in the study of thin structures using a stabilized finite element method applied to solid-shell elements. This type of elements are subject to all kinds of numerical locking when approximated using the standard irreducible Galerkin approach and low order elements. Therefore, all the locking effects have to be properly evaluated; these are:

- Shear locking is usually described in the classical shell context as the inability of a thin structure to represent zero bending strains [2]. In the context of solid-shell elements, it appears when the shell is not able to reproduce a correct coupling between the in-plane translation of its upper and lower surfaces with respect to the transverse translation of the mid-surface. For this reason, shear-locking is present in flat and curved structures subject to bending states, and the effect becomes greater as the thickness gets smaller. As a consequence of this, parasitic transverse shear strains cause an over-stiffening of the structure, leading to spurious results.

- Membrane locking appears due to the inability of the shell to reproduce the coupling between the in-plane translation of its upper and lower surfaces with respect to the in-plane translation of the mid-surface. Obviously, this implies that membrane locking only appears in curved structures [22]. In this case this locking manifests itself as parasitic membrane strains when subject to inextensional bending deformations, leading to increased stiffening of the structure as well, and the locking effect intensifies as the structure gets thinner.

- Poisson thickness locking occurs when through-the-thickness displacement is approximated linearly in a bending state. The linear approximation implies that the normal transverse strains get approximated as a constant. At the same time, the in-plane strains vary linearly in the thickness direction. Normal transverse and in-plane strains are coupled through Poisson's ratio. Therefore, locking arises due to the incompatibility of the approximation between the constant normal transverse strain coupled with in-plane strains which vary linearly in the transverse direction. The locking effect is only proportional to Poisson's ratio and is not affected by the thickness of the structure.

- Trapezoidal locking occurs in solid-shell elements when the shell directors defined by the element edges are not parallel [23]. It creates parasitic normal transverse strains due to the faulty coupling between the in-plane bending and the transverse extension of the element.

- Volumetric locking occurs when the material is incompressible or approaches incompressibility. The material bulk modulus increases uncontrollably and, since it scales the volumetric strains, it creates parasitic strains in the normal directions. Therefore it affects the membrane in-plane and the normal thickness strains [21].

A vast amount of research has been done with the objective of solving all kinds of numerical locking in the solid-shell context. The locking effects are mostly due to parasitic strains in a specific direction, and different approaches were focused on treating each one of them individually.

One of the most influential approaches was the Assumed Strain (AS) method, first developed by MacNeal in [24] for classic shell theory problems. It was followed by Assumed Natural Strain (ANS) methods [25]. Another important contribution to the subject was introduced by Simo and Hughes in [26] using a variational framework, which led to the Enhanced Assumed Strains (EAS) method [27]. These approaches were eventually adopted for solid-shell elements [28]. Notable developments were done by Klinkel et al [29] using ANS and EAS in linear and finite strain problems, and by Sze et al. using ANS [30, 31] to solve linear and non-linear problems, and using EAS [32] to solve hyperelastic problems. The AS, ANS and EAS approaches have endured through time, and can be found in more recent literature. Kim et al. [33] used the ANS method together with a Resultant Force formulation to solve solid-shell in finite strain problems. Hajlaoui et al. [34] developed a high order solid-shell element based on the EAS to solve buckling in solid-shell problems, and used ANS in the thickness direction to avoid locking effects. Mostafa et al. [35] used a combination of ANS and EAS to deal with all types of numerical locking independently, and solved non-linear problems. Caseiro et al. [36] extended the ANS approach to NURBS based formulations

to alleviate shear and membrane locking effects in linear analysis and then extended the approach to non-linear problems [37]. More recently, Huang et al. [38] developed a solid-shell element using the ANS concept in the unsymmetric finite element method.

Another common approach is the use of Reduced Integration (RI), first implemented in classical shell theory [39, 40, 41]. The method has found success over the years; however it can lead to spurious zero energy modes, known as hourglassing [42], that need to be stabilized. This is most commonly approached in the literature through assumed strain methods [22]. In this context, Schwarze and Reese used the ANS and EAS approach together with reduced integration and hourglass stabilization to solve linear [43] and finite strain [44] solid-shell problems. Reese [45] worked in a RI approach based in the EAS concept to implement a hourglass stabilization to solve large strain shell problems. Pagani et al. [46] used a RI based solid-shell formulation stabilized with ANS and EAS to solve explicit non-linear problems with selective mass scaling to achieve large critical time steps. The reduced integration approach is still being developed in the solid-shell framework. Leonetti et al. [47] proposed a model based in a combination of linear integration in the thickness direction and NURBS interpolation in the mid-plane that has been successfully used in non-linear problems. Barfusz et al. [48] used a RI based solid-shell element stabilized with ANS and EAS methods to avoid numerical locking, and solved damage plasticity problems with the resulting method.

The Mixed Interpolated Tensorial Components (MITC) method has also proven to be an effective approach to avoid numerical locking [49, 50]. The earlier contributions of this approach come from Dvokin and Bathe [51] in classical shell elements, and it has been studied further ever since [52, 53, 54]. Important contributions to the subject have been developed in solid-shell elements by Chapelle et al. [55]. The MITC approach has been one of the major approaches in the solid-shell framework. Sussman and Bathe [56] developed a MITC approach in solid-shell problems to avoid numerical locking, using nodal control vectors to describe large deformations. Recent publications show prominent results using the MITC approach in three-dimensional shell problems. Cinefra [57] solved linear solid-shell problems in curvilinear coordinates using MITC in each local strain component to solve numerical locking. Rezaiee et al. [58] used the MITC and ANS approaches together with the arc-length method to solve functionally graded shells in non-linear large deformations problems.

Many other methods have also been employed to solve locking problems, such as the B-bar method. It was first introduced by Hughes in [59] for classic shell theory using linear elements, and it was later developed in solid-shells by Simo et al. [60] using a mixed formulation for stresses formulated with a volumetric-deviatoric split. Hybrid-strain and hybrid-stress methods have also been developed for solid-shell elements in the linear [61, 62] and non-linear regimes [63, 64].

The present work deals with numerical locking in solid-shell problems *introducing additional stresses as new unknowns*, thus leading to a problem whose unknowns are stresses and displacements. The first issue to analyze is how to deal with this mixed problem, i.e., how to treat the possible compatibility conditions between the interpolation of stresses and displacements. We avoid the need to satisfy any of such conditions by using a stabilized finite element formulation based on the Variational Multiscale (VMS) framework, first introduced by Hughes [65, 66] and later developed in [67, 68]. In particular, this method allows us to use equal interpolation for stresses and displacements. Other problems that involve stresses as variables are viscoelastic flows [69, 70] or mixed formulations in solid mechanics [71, 72] (see also [73]).

The second issue to consider is *which* stresses need to be introduced as unknowns. For that, we need to have the *mechanical meaning* of the components of the stress tensor, independently of the global reference system chosen. To this end, we shall write the equilibrium equations in a curvilinear system associated to the shell, with two tangent orthogonal coordinates and a normal one. This will allow us to interpret the stress components as shear, twisting, membrane and thickness stresses. Then, a variety of benchmark cases will determine which of these stresses are required to avoid the different types of numerical locking that can appear. This systematic study is, to our knowledge, completely new. Let us anticipate that the conclusion of our analysis is that *there are situations in which each of the stress components is necessary to avoid locking.*

In this work we will restrict ourselves to linear elasticity, under the infinitesimal strain assumption. Finite strains and hyperelastic materials will be considered in Part II. From the results of the present paper, all the stress components and the displacements will be considered as unknowns in this second paper.

This paper is organized as follows. First, we describe the geometrical ingredients to write the elasticity equations in curvilinear coordinates (Section 2) and later we write these equations (to fix notation), both in differential and variational forms (Section 3). The geometrical approximation of the problem is explained in Section 4, and the finite element approximation in Section 5. The numerical experimentation is presented in Section 6 and conclusions are drawn in Section 7.

2. Linear elasticity using curvilinear coordinates

This section collects basic results of the theory of elasticity expressed in general curvilinear coordinates (further details can be found in book by Washizu [74]). Regarding the notation employed, Greek indices will correspond to curvilinear coordinates, whereas lower case Latin indices to Cartesian coordinates.

2.1. Geometrical description

Let us consider a system of curvilinear coordinates $(\theta^1, \theta^2, \theta^3)$; under the infinitesimal stress assumption, the geometry of the initial and the deformed configurations will be considered equal. The position vector of any point P of curvilinear coordinates $(\theta^1, \theta^2, \theta^3)$ will be given by

$$\boldsymbol{x} = \boldsymbol{x}(\theta^1, \theta^2, \theta^3) = x^i \boldsymbol{e}_i,$$

where $\boldsymbol{e}_i$, $i = 1, 2, 3$, is the i-th vector of the Cartesian basis and $x^i = x^i(\theta^1, \theta^2, \theta^3)$, $i = 1, 2, 3$ are the functions that relate the curvilinear and the Cartesian coordinates. Here and below, Einstein's summation convention is used, with repeated indexes summing from 1 to 3.

Let the notation $(\cdot)_{,\alpha}$ be the differentiation respect to θ^α, namely $(\cdot)_{,\alpha} = \partial(\cdot)/\partial\theta^\alpha$. The covariant base vectors associated to point P are defined as

$$\boldsymbol{g}_\alpha = \frac{\partial \boldsymbol{x}}{\partial \theta^\alpha} = \boldsymbol{x}_{,\alpha}, \quad \alpha = 1, 2, 3. \tag{2.1}$$

The covariant base vectors allow the definition of the covariant metric tensor $g_{\alpha\beta}$ as

$$g_{\alpha\beta} = \boldsymbol{g}_\alpha \cdot \boldsymbol{g}_\beta, \quad \alpha, \beta = 1, 2, 3, \tag{2.2}$$

the contravariant metric tensor $g^{\alpha\beta}$ being its inverse, i.e.,

$$g_{\alpha\gamma} g^{\gamma\beta} = \delta^\alpha_\beta, \tag{2.3}$$

where δ^α_γ is the Kronecker symbol. This allows us to define the contravariant base vectors as

$$\boldsymbol{g}^\alpha = g^{\alpha\beta} \boldsymbol{g}_\beta. \tag{2.4}$$

The derivatives of covariant vectors respect to θ^α can be obtained as

$$\boldsymbol{g}_{\alpha,\beta} = (\boldsymbol{x}_{,\alpha})_{,\beta} = (\boldsymbol{x}_{,\beta})_{,\alpha} = \boldsymbol{g}_{\beta,\alpha}. \tag{2.5}$$

Additionally, let $\Gamma^\gamma_{\alpha\beta}$ be the three index Christoffel symbol of second kind, which provide a measure of the curvature of the coordinate axes through space, defined as

$$\Gamma^\gamma_{\alpha\beta} = \boldsymbol{g}_{\alpha,\beta} \cdot \boldsymbol{g}^\gamma = -\boldsymbol{g}^\gamma_{,\alpha} \cdot \boldsymbol{g}_\beta. \tag{2.6}$$

The Christoffel symbols allow us to write the derivatives of the covariant and contravariant base vectors as:

$$\boldsymbol{g}_{\alpha,\beta} = \Gamma^\gamma_{\alpha\beta} \boldsymbol{g}_\gamma, \quad \boldsymbol{g}^\alpha_{,\beta} = -\Gamma^\alpha_{\gamma\beta} \boldsymbol{g}^\gamma.$$

Consider next a vector field in space $\boldsymbol{u}\left(\theta^1, \theta^2, \theta^3\right)$. This can be written both in terms of the covariant components u_α or contravariant components u^α as

$$\boldsymbol{u} = u^\alpha \boldsymbol{g}_\alpha = u_\alpha \boldsymbol{g}^\alpha. \tag{2.7}$$

By using the definition in equation (2.6), the differentiation of $\boldsymbol{u}$ respect to θ^β results in

$$\begin{aligned}
\boldsymbol{u}_{,\beta} &= \left(u^\alpha \boldsymbol{g}_\alpha\right)_{,\beta} && = \left(u_\alpha \boldsymbol{g}^\alpha\right)_{,\beta} \\
&= u^\alpha{}_{,\beta} \boldsymbol{g}_\alpha + u^\alpha \boldsymbol{g}_{\alpha,\beta} && = u_{\alpha,\beta} \boldsymbol{g}^\alpha + u_\alpha \boldsymbol{g}^\alpha{}_{,\beta} \\
&= u^\alpha{}_{,\beta} \boldsymbol{g}_\alpha + u^\alpha \Gamma^\gamma_{\alpha\beta} \boldsymbol{g}_\gamma && = u_{\alpha,\beta} \boldsymbol{g}^\alpha - u_\alpha \Gamma^\alpha_{\gamma\beta} \boldsymbol{g}^\gamma \\
&= u^\alpha{}_{|\beta} \boldsymbol{g}_\alpha && = u_{\alpha|\beta} \boldsymbol{g}^\alpha
\end{aligned} \tag{2.8}$$

where $(\cdot)_{|\beta}$ represents the covariant differentiation of the vector component. It can be obtained either for the

covariant or contravariant components of a vector field, respectively as

$$u^{\alpha}{}_{|\beta} = u^{\alpha}{}_{,\beta} + u^{\gamma}\Gamma^{\alpha}_{\gamma\beta}, \qquad u_{\alpha|\beta} = u_{\alpha,\beta} - u_{\gamma}\Gamma^{\gamma}_{\alpha\beta}.$$

2.2. Transformation of the stress and the strain tensors

Let us obtain the transformation rule of the stress and the strain tensors between their Cartesian components written in terms of the Cartesian coordinates $\left(x^1, x^2, x^3\right)$ and their curvilinear components written in terms of the curvilinear coordinates $(\theta^1, \theta^2, \theta^3)$. Differentiation respect to θ^α and x^i, $\alpha, i = 1, 2, 3$, can be related using the chain rule as

$$\frac{\partial(\ )}{\partial\theta^\alpha} = \frac{\partial(\ )}{\partial x^i}\frac{\partial x^i}{\partial\theta^\alpha}, \qquad \frac{\partial(\ )}{\partial x^i} = \frac{\partial(\ )}{\partial\theta^\alpha}\frac{\partial\theta^\alpha}{\partial x^i}.$$

Making use of this and equation (2.1) it becomes clear that

$$\boldsymbol{g}_\alpha = \frac{\partial\boldsymbol{x}}{\partial\theta^\alpha} = \frac{\partial\boldsymbol{x}}{\partial x^i}\frac{\partial x^i}{\partial\theta^\alpha} = \frac{\partial x^i}{\partial\theta^\alpha}\boldsymbol{e}_i, \tag{2.9}$$

and

$$\boldsymbol{e}_i = \frac{\partial\boldsymbol{x}}{\partial x^i} = \frac{\partial\boldsymbol{x}}{\partial\theta^\alpha}\frac{\partial\theta^\alpha}{\partial x^i} = \frac{\partial\theta^\alpha}{\partial x^i}\boldsymbol{g}_\alpha. \tag{2.10}$$

Scalar multiplication of equation (2.9) by $\boldsymbol{e}^i \equiv \boldsymbol{e}_i$ yields

$$\frac{\partial x^i}{\partial\theta^\alpha} = \boldsymbol{e}^i \cdot \boldsymbol{g}_\alpha, \tag{2.11}$$

and similarly, scalar multiplication of equation (2.10) by $\boldsymbol{g}^\alpha$ yields

$$\frac{\partial\theta^\alpha}{\partial x^i} = \boldsymbol{e}_i \cdot \boldsymbol{g}^\alpha. \tag{2.12}$$

For the variables in curvilinear coordinates, consider the displacement vector field $\boldsymbol{u}$, the second order stress and strain fields $\boldsymbol{\sigma}$ and $\boldsymbol{\varepsilon}$, respectively, and the fourth order elasticity tensor $\mathbb{C}$. Let the variables in the Cartesian basis be represented as $\hat{(\cdot)}$, assumed to be expressed in terms of the Cartesian coordinates. As detailed in [74], it follows that the transformation laws between Cartesian and curvilinear coordinates are:

$$\hat{\sigma}^{ij} = \frac{\partial x^i}{\partial\theta^\alpha}\frac{\partial x^j}{\partial\theta^\beta}\sigma^{\alpha\beta}, \tag{2.13}$$

$$\hat{\varepsilon}_{ij} = \frac{\partial\theta^\alpha}{\partial x^i}\frac{\partial\theta^\beta}{\partial x^j}\varepsilon_{\alpha\beta}, \tag{2.14}$$

$$\hat{u}_i = \frac{\partial\theta^\alpha}{\partial x^i}u_\alpha, \tag{2.15}$$

$$\hat{\mathbb{C}}^{ijkl} = \frac{\partial x^i}{\partial\theta^\alpha}\frac{\partial x^j}{\partial\theta^\beta}\frac{\partial x^k}{\partial\theta^\gamma}\frac{\partial x^l}{\partial\theta^\delta}\mathbb{C}^{\alpha\beta\gamma\delta}. \tag{2.16}$$

The inverse transformation rules are

$$\sigma^{\alpha\beta} = \frac{\partial\theta^\beta}{\partial x^j}\frac{\partial\theta^\alpha}{\partial x^i}\hat{\sigma}^{ij}, \tag{2.17}$$

$$\varepsilon_{\alpha\beta} = \frac{\partial x^j}{\partial\theta^\beta}\frac{\partial x^i}{\partial\theta^\alpha}\hat{\varepsilon}_{ij}, \tag{2.18}$$

$$u_\alpha = \frac{\partial x^i}{\partial\theta^\alpha}\hat{u}_i, \tag{2.19}$$

$$\mathbb{C}^{\alpha\beta\gamma\delta} = \frac{\partial\theta^\delta}{\partial x^l}\frac{\partial\theta^\gamma}{\partial x^k}\frac{\partial\theta^\beta}{\partial x^j}\frac{\partial\theta^\alpha}{\partial x^i}\hat{\mathbb{C}}^{ijkl}. \tag{2.20}$$

We shall come back to some of these transformations later on.

Figure 1 represents the stress components in both the curvilinear and the Cartesian bases, in this case both seen from the Cartesian reference system. As usual, this representation is done on an element of solid, now considering that it is thin in one direction, namely, that of θ^3 in curvilinear coordinates (see below). The key idea is that if

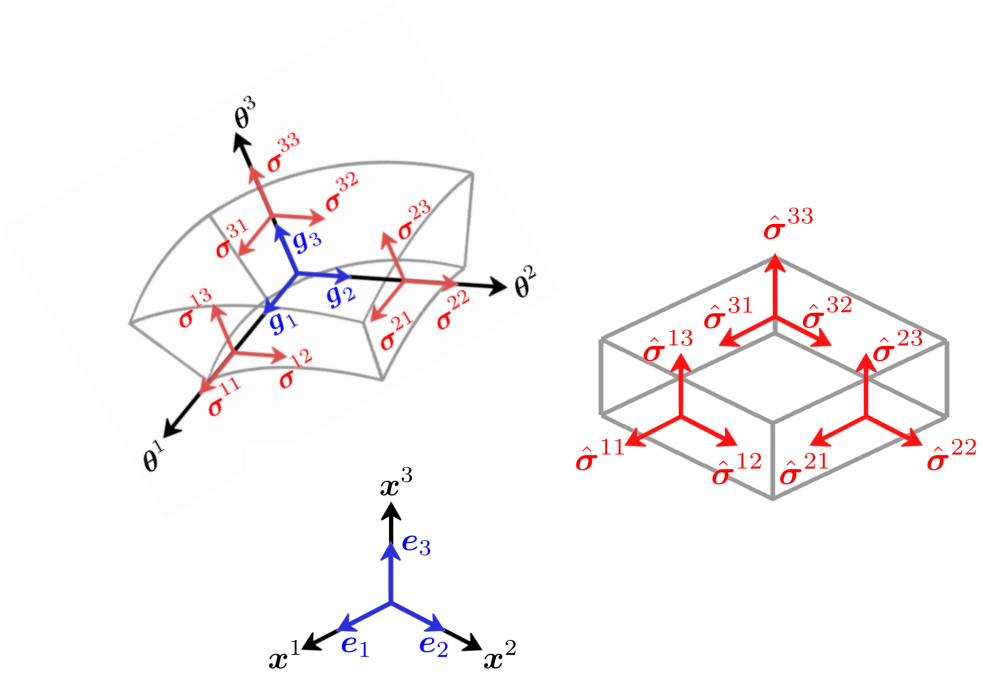

Figure 1: Notation for the stress components. In curvilinear coordinates, the stresses can be grouped as follows: σ^{11}, σ^{22} are the membrane stresses; $\sigma^{12} = \sigma^{21}$ are the twisting stresses; $\sigma^{13} = \sigma^{31}$, $\sigma^{23} = \sigma^{32}$ are the shear stresses; σ^{33} is the transverse stress. In Cartesian coordinates, this physical interpretation is not possible.

we consider that the solid is a shell whose mid surface is parametrized by θ^1 and θ^2, we can provide of mechanical meaning the stress components in curvilinear coordinates, but not in Cartesian coordinates. Indeed, in the situation represented in Fig. 1, σ^{11} and σ^{22} are the membrane stresses (the stresses tangent to the shell), $\sigma^{12} = \sigma^{21}$ are the twisting stresses (the stresses that cause rotation on the planes tangent to the shell), $\sigma^{13} = \sigma^{31}$, $\sigma^{23} = \sigma^{32}$ are the shear stresses (stresses on the faces of the solid element perpendicular to the shell and pointing in the perpendicular direction) and σ^{33} is the transverse stress (the stress on the shell surface and normal to it). This mechanical interpretation is not possible in Cartesian coordinates.

3. Governing equations

3.1. Differential form

Let us write the governing equations for the linear elasticity problem in a frame invariant (intrinsic) form. This will serve us to introduce the notation employed in the finite element approximation of the problem. Consider Ω to be the domain occupied by the solid in $\mathbb{R}^3$ and $\partial\Omega$ its boundary. The static equations of motion, the constitutive equations for stress, and the kinematic equations for the strain-displacement relationship are written, respectively, as

$$-\nabla \cdot \boldsymbol{\sigma} = \rho \boldsymbol{b} \qquad \text{in } \Omega, \tag{3.1}$$

$$\boldsymbol{\sigma} - \mathbb{C} : \boldsymbol{\varepsilon} = \mathbf{0} \qquad \text{in } \Omega, \tag{3.2}$$

$$\boldsymbol{\varepsilon} - \nabla^s \boldsymbol{u} = \mathbf{0} \qquad \text{in } \Omega, \tag{3.3}$$

where ρ is the density, $\boldsymbol{b}$ are the body forces per unit of mass, and $\nabla^s \boldsymbol{u}$ is the symmetric gradient of the displacement.

Additional notation is necessary to build the formulations below. Let us define, in a general manner, a linear differential operator $\mathcal{L}$, the associated trace operator $\mathcal{D}$ that makes the following problem well defined, and a external force vector $\boldsymbol{F}$. Consider $\boldsymbol{U}$ to be the unknown of n components of the problem, to be defined for each specific formulation. The solid mechanics problem can be written in an abstract form as the problem of finding $\boldsymbol{U} : \Omega \to \mathbb{R}^n$

such that

$$\mathcal{L}\boldsymbol{U} = \boldsymbol{F} \qquad \text{in } \Omega, \tag{3.4}$$

$$\mathcal{D}\boldsymbol{U} = \bar{\boldsymbol{U}} \qquad \text{on } \partial\Omega. \tag{3.5}$$

We will consider $\bar{\boldsymbol{U}} = \boldsymbol{0}$ for simplicity.

Let us consider first the irreducible form of the solid problem in terms of the displacements, by replacing the strain in equation (3.3) into equation (3.2), and replacing the stress into equation (3.1). The strong form of the problem reduces to finding the unknown $\boldsymbol{U} = \boldsymbol{u}$, and now the linear operator and the external forces vector take the form $\mathcal{L} = \mathcal{L}_u$ and $\boldsymbol{F}_u$, respectively, where

$$\mathcal{L}_u\boldsymbol{u} = -\nabla\cdot\mathbb{C}:\nabla^s\boldsymbol{u}, \qquad \boldsymbol{F}_u = \rho\boldsymbol{b}.$$

In this case, $n = 3$ and $\mathcal{D}\boldsymbol{U} = \boldsymbol{u}$.

As for the mixed form of the problem, the two field displacement-stress approach is formulated by considering equations (3.1)-(3.3) and replacing the strains from equations (3.3) into equation (3.2). The mixed problem reduces to finding the unknown $\boldsymbol{U} = [\boldsymbol{u}, \boldsymbol{\sigma}]$, and now the linear operator and the external forces vector take the form $\mathcal{L} = \mathcal{L}_{\sigma u}$ and $\boldsymbol{F}_{\sigma u}$, respectively, where

$$\mathcal{L}_{\sigma u}\boldsymbol{U} = \begin{bmatrix} -\nabla\cdot\boldsymbol{\sigma} \\ \boldsymbol{\sigma} - \mathbb{C}:\nabla^s\boldsymbol{u} \end{bmatrix}, \qquad \boldsymbol{F}_{\sigma u} = \begin{bmatrix} \rho\boldsymbol{b} \\ \boldsymbol{0} \end{bmatrix},$$

and $\mathcal{D}[\boldsymbol{u}, \boldsymbol{\sigma}] = \boldsymbol{u}$. The problem can be symmetrized by writing the second equation as $\mathbb{C}^{-1} : \boldsymbol{\sigma} - \nabla^s\boldsymbol{u} = \boldsymbol{0}$. In this case, $n = 3 + 6 = 9$ if the symmetry of the stress tensor is taken into account in the trial and test spaces and imposed strongly, and $n = 3 + 9 = 12$ if it is not and this symmetry is a consequence of the constitutive law (which will be imposed weakly in the finite element approximation). In our implementation, we impose the symmetry of $\boldsymbol{\sigma}$ strongly.

3.2. Variational form

Consider $H^1(\Omega)$ to be the space of functions in $L^2(\Omega)$ whose derivatives belong to $L^2(\Omega)$. We denote as $\mathcal{U} = H^1(\Omega)^3$ the space of displacements and as $\mathcal{S} = L^2(\Omega)^{3\times3}_{\text{sym}}$ the space of stresses. As said above, the symmetry of the latter can be enforced strongly in the trial space or weakly through the weak form of the constitutive equation (see below). Let $\mathcal{X}$ be the space where the weak problem is defined, being $\mathcal{X} = \mathcal{U}$ in the case of the irreducible formulation and $\mathcal{X} = \mathcal{U} \times \mathcal{S}$ in the case of the mixed formulation; the tests functions are $\boldsymbol{V} = \boldsymbol{v} \in \mathcal{X}$ and $\boldsymbol{V} = [\boldsymbol{v}, \boldsymbol{\tau}] \in \mathcal{X}$, respectively. Let us introduce the bilinear form B and the linear form L as

$$B(\boldsymbol{V}, \boldsymbol{U}) = \begin{cases} (\nabla^s\boldsymbol{v}, \mathbb{C}:\nabla^s\boldsymbol{u}) & \text{in the irreducible case,} \\ (\nabla^s\boldsymbol{v}, \boldsymbol{\sigma}) + (\boldsymbol{\tau}, \mathbb{C}^{-1}:\boldsymbol{\sigma}) - (\boldsymbol{\tau}, \nabla^s\boldsymbol{u}) & \text{for the stress-displacement formulation,} \end{cases}$$

$$L(\boldsymbol{V}) = \langle \boldsymbol{V}, \boldsymbol{F} \rangle,$$

where $(\cdot,\cdot)$ represents the inner product in $L^2(\Omega)$ and $\langle\cdot,\cdot\rangle$ the integral of the multiplication of two functions in Ω. When there are traction boundary conditions, these should appear in the expression of the linear form L.

With all the above, the general form of the problem in equations (3.4) and (3.5) can be written in its weak form, which consists of finding $\boldsymbol{U} \in \mathcal{X}$ such that

$$B(\boldsymbol{V}, \boldsymbol{U}) = L(\boldsymbol{V}), \tag{3.6}$$

for all $\boldsymbol{V} \in \mathcal{X}$.

4. Geometrical approximation using finite elements

4.1. Construction of the local basis

Let us consider the shell represented by a surface $\Omega^{2\text{D}}$ in $\mathbb{R}^3$, geometrically expressed by any means. Suppose that we have a finite element partition $\mathcal{T}_h = \{K\}$ of $\Omega^{2\text{D}}$ of diameter h, so that $\bar{\Omega}^{2\text{D}} = \bigcup_{K\in\mathcal{T}_h} K$. We will not consider the error stemming from the geometrical approximation of the shell, and thus we will consider this finite element

representation as exact. Let $K \in \mathcal{T}_h$ be an element domain of the partition, either simplicial or a quadrilateral, and consider the isoparametric mapping

$$\begin{aligned} \boldsymbol{\varphi}_K : K_0 &\longrightarrow K \\ (\xi, \eta) &\mapsto (x^1, x^2, x^3), \end{aligned}$$

that maps the reference domain $K_0 \subset \mathbb{R}^2$ to $K \subset \mathbb{R}^3$, (ξ, η) being the isoparametric coordinates. Considering a Lagrangian interpolation, if n_{nod} is the number of nodes of K and $N^A(\xi, \eta)$ are the shape functions on K_0, $A = 1, \ldots, n_{\text{nod}}$, we have that

$$\boldsymbol{\varphi}_K(\xi, \eta) = \sum_{A=1}^{n_{\text{nod}}} N^A(\xi, \eta) \boldsymbol{x}^A,$$

where $\boldsymbol{x}^A$ is the position vector of node A in K, $A = 1, \ldots, n_{\text{nod}}$. The collection of all mappings $\{\boldsymbol{\varphi}_K, K \in \mathcal{T}_h\}$ provides a local parametrization of Ω^{2D}.

The vectors tangent to each $K \in \mathcal{T}_h$ are given by

$$\begin{aligned} \boldsymbol{g}^*_{1,K} &= \left| \frac{\partial \boldsymbol{\varphi}_K}{\partial \xi} \right|^{-1} \frac{\partial \boldsymbol{\varphi}_K}{\partial \xi}, \quad \frac{\partial \boldsymbol{\varphi}_K}{\partial \xi} = \sum_{A=1}^{n_{\text{nod}}} \frac{\partial N^A}{\partial \xi} \boldsymbol{x}^A, \\ \boldsymbol{g}^*_{2,K} &= \left| \frac{\partial \boldsymbol{\varphi}_K}{\partial \eta} \right|^{-1} \frac{\partial \boldsymbol{\varphi}_K}{\partial \eta}, \quad \frac{\partial \boldsymbol{\varphi}_K}{\partial \eta} = \sum_{A=1}^{n_{\text{nod}}} \frac{\partial N^A}{\partial \eta} \boldsymbol{x}^A. \end{aligned}$$

From them, we can compute a vector normal to $K \subset \Omega^{\text{2D}}$ as

$$\boldsymbol{g}^*_{3,K} = \boldsymbol{g}^*_{1,K} \times \boldsymbol{g}^*_{2,K}.$$

Note that $|\boldsymbol{g}^*_{3,K}| = 1$ if ξ and η are orthogonal coordinates, as it is usually the case; otherwise, we normalize $\boldsymbol{g}^*_{3,K}$. It is important to remark that this normalization is not necessary, although we will construct the basis vectors to be orthonormal. The implication of this is that the metric tensor will be the identity; however, we shall consider its expression in the case of arbitrary local basis, for generality.

The basis vectors constructed this way, $\{\boldsymbol{g}^*_{1,K}, \boldsymbol{g}^*_{2,K}, \boldsymbol{g}^*_{3,K}\}$, are discontinuous across elements. To construct a continuous basis we proceed as follows. First, the vector field $\boldsymbol{g}^*_{3,K}$, $K \in \mathcal{T}_h$, is projected onto the space of continuous vector fields using a standard $L^2(\Omega^{\text{2D}})$ projection, thus obtaining the nodal vectors $\boldsymbol{g}^a_3$, $a = 1, \ldots, n_{\text{pts}}$, n_{pts} being the nodal points of $\mathcal{T}_h$, and, from them

$$\boldsymbol{g}_3(x^1, x^2, x^3) = G_3^{-1} \sum_{a=1}^{n_{\text{pts}}} N^a(x^1, x^2, x^3) \boldsymbol{g}^a_3, \quad G_3 = |\sum_{a=1}^{n_{\text{pts}}} N^a(x^1, x^2, x^3) \boldsymbol{g}^a_3|,$$

N^a being the global shape function of node a. Within each element $K \in \mathcal{T}_h$, if A is the local numbering of the global node a, we have :

$$\boldsymbol{g}_3|_K(\xi, \eta) = G_{3,K}^{-1} \sum_{A=1}^{n_{\text{nod}}} N^A(\xi, \eta) \boldsymbol{g}^A_{3,K}, \quad G_{3,K} = |\sum_{A=1}^{n_{\text{nod}}} N^A(\xi, \eta) \boldsymbol{g}^A_{3,K}|. \tag{4.1}$$

Figure 2 shows a cut of a surface and the conceptual difference between $\boldsymbol{g}^*_{3,K}$ and $\boldsymbol{g}_3$ when linear elements are used, case in which $\boldsymbol{g}^*_{3,K}$ will be constant on each $K \in \mathcal{T}_h$.

Once the continuous global vector field $\boldsymbol{g}_3$ is constructed, we can build the a continuous local basis at each point $\{\boldsymbol{g}_1, \boldsymbol{g}_2, \boldsymbol{g}_3\}$ by defining

$$\boldsymbol{g}_1 = |\boldsymbol{g}_3 \times \boldsymbol{e}_3|^{-1} \boldsymbol{g}_3 \times \boldsymbol{e}_3, \quad \boldsymbol{g}_2 = \boldsymbol{g}_3 \times \boldsymbol{g}_1, \tag{4.2}$$

the only exception being when $\boldsymbol{g}_3$ aligns with $\boldsymbol{e}_3$, case in which we set $\boldsymbol{g}_1 = \boldsymbol{e}_1$ and $\boldsymbol{g}_2 = \boldsymbol{e}_2$ (or changing the sign if $\boldsymbol{g}_3$ is opposite to $\boldsymbol{e}_3$). The covariant basis $\{\boldsymbol{g}_1, \boldsymbol{g}_2, \boldsymbol{g}_3\}$ constructed this way will be such that $\{\boldsymbol{g}_1, \boldsymbol{g}_2\}$ will be *approximately* tangent to Ω^{2D} and $\boldsymbol{g}_3$ *approximately* normal. In fact, we can consider the shell defined by $\{\boldsymbol{g}_1, \boldsymbol{g}_2, \boldsymbol{g}_3\}$. The curvilinear coordinates $(\theta^1, \theta^2, \theta^3)$ are then defined as those tangent to $\{\boldsymbol{g}_1, \boldsymbol{g}_2, \boldsymbol{g}_3\}$ at each point.

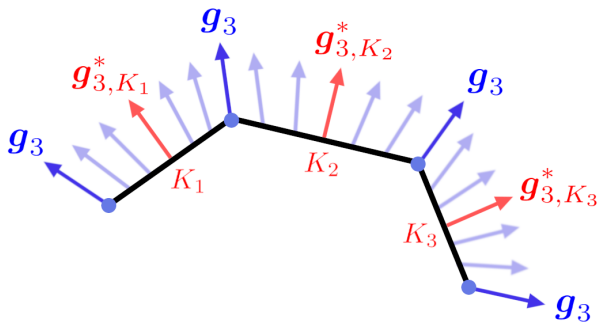

Figure 2: Normal vectors to the shell $\boldsymbol{g}^*_{3,K}$ and their smoothing $\boldsymbol{g}_3$.

4.2. Extrusion of the shell mid-surface

The domain Ω^{2D} (or, in fact, its approximation associated to $\{\boldsymbol{g}_1, \boldsymbol{g}_2, \boldsymbol{g}_3\}$) will be considered as the mid-surface of the shell. The solid-shell domain where the calculations will be performed is denoted as Ω^{3D}, and it is computed from the extrusion of Ω^{2D} in the normal direction. As we shall see, the construction of Ω^{3D} can be done element-wise because of the continuity of $\boldsymbol{g}_3$.

Suppose that the thickness of the shell is defined by its values at the nodes of $\mathcal{T}_h$, denoted as t^a, $a = 1, \dots n_{\text{pts}}$. For each $K \in \mathcal{T}_h$, the thicknesses at the nodes will be t^A_K, A being the local number of node a, and we can construct the thickness function

$$t_K(\xi, \eta) = \sum_{A=1}^{n_{\text{nod}}} N^A(\xi, \eta) t^A_K.$$

From the reference element K_0 we can construct the 3D reference element $K^{3D}_0 = K_0 \times [-1, 1]$ and the mapping

$$\begin{aligned} &\boldsymbol{\psi}_K : K^{3D}_0 \longrightarrow \mathbb{R}^3 \\ &\quad (\xi, \eta, \zeta) \mapsto (x^1, x^2, x^3) = \boldsymbol{\varphi}_K(\xi, \eta) + \zeta \frac{1}{2} t_K(\xi, \eta) \boldsymbol{g}_3|_K(\xi, \eta). \end{aligned} \tag{4.3}$$

and then set $K^{3D} = \boldsymbol{\psi}_K(K^{3D}_0)$, i.e., the image of K^{3D}_0 through $\boldsymbol{\psi}_K$. The solid domain where the problem is posed is then

$$\Omega^{3D} = \bigcup_{K \in \mathcal{T}_h} K^{3D}.$$

From the continuity of $\boldsymbol{g}_3$ and the intrinsic continuity of the thickness function, Ω^{3D} will be a smooth extrusion of Ω^{2D}. This domain, together with the systems of coordinates and basis introduced so far, are depicted in Fig. 3. In the following, we will consider only one element across the thickness, but the extension to an arbitrary number of elements is straightforward, simply by fixing a partition of the thickness t_K in equations (4.3).

We could now extend the construction of the local basis $\{\boldsymbol{g}^*_{1,K}, \boldsymbol{g}^*_{2,K}, \boldsymbol{g}^*_{3,K}\}$ from K to K^{3D}. In general, the resulting vectors will depend on the coordinate ζ because of the dependence of t_K and $\boldsymbol{g}_3|_K$ on (ξ, η), which will need to be taken into account when computing $\boldsymbol{g}^*_{1,K}$ and $\boldsymbol{g}^*_{2,K}$ (see equation (4.3)). However, since we are interested in solids of small thickness, we shall take the basis $\{\boldsymbol{g}_1, \boldsymbol{g}_2, \boldsymbol{g}_3\}$ as constant across the thickness of the shell.

4.3. Interpolation across the thickness

Once the element domains $\{K^{3D}\}$ have been constructed, we need to define their degrees of freedom and a basis for the finite element space we wish to construct. As for the original partition $\{K\}$, we shall consider continuous Lagrangian interpolations, and it suffices to define them for the reference element $K_0 \times [-1, 1]$. Precisely, one of the main reasons to use 3D solid elements in the approximation of shell structures in to take advantage of the through-the-thickness interpolation of the unknowns. For this reason, it is convenient that the discretization of the mesh is performed considering an independent discretization in the thickness direction. In other words, the number of elements, the order of interpolation, and the integration rule are set independently from the original surface mesh.

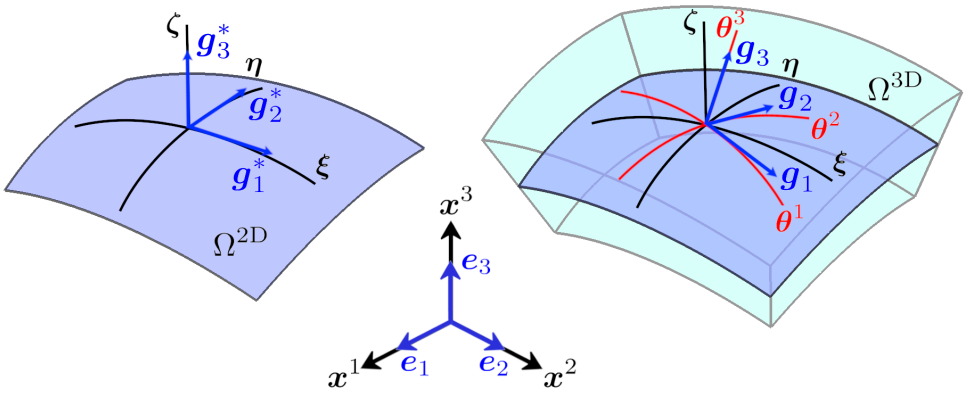

Figure 3: Geometry of the shell: 2D surface (left) and 3D extruded volume (right).

Let n_s be the interpolation order of $K \in \mathcal{T}_h$ and n_l the interpolation order of the elements in the ζ direction of the reference element. Let $N_i^{A,A'}(\xi,\eta,\zeta)$ be the shape function of a node in $K_0 \times [-1,1]$ that corresponds to node A of K_0 and node A' of the discretization of $[-1,1]$. The shape functions corresponding to the shell body $N_i^{A,A'}(\xi,\eta,\zeta)$ can now be constructed by multiplying the mid-surface shape functions $N^A(\xi,\eta)$ and the standard one dimensional Lagrangian shape functions $N^{A'}(\zeta)$ in the isoparametric space:

$$N^{A,A'}(\xi,\eta,\zeta) = N^A(\xi,\eta)\, N^{A'}(\zeta)\,. \tag{4.4}$$

Possible interpolations of hexahedral elements are shown in Table 1 for $n_s = 1,2$ and $n_l = 1,2$. In the following, the structure of the shape functions will be assumed and we shall simply write as $N^A(\xi,\eta,\zeta)$ the local shape function of node A, not necessarily in $K \in \mathcal{T}_h$ but in K^{3D}; the number of nodes of K^{3D} will be again denoted as n_{nod}. Likewise, at the global level the shape functions will be written as $N^a(x^1,x^2,x^3)$, with a running again from 1 to n_{pts}. The finite element partition resulting from the extrusion of the finite element partition of the shell surface $\mathcal{T}_h = \{K\}$ will be denoted as $\mathcal{T}_h^{3D} = \{K^{3D}\}$.

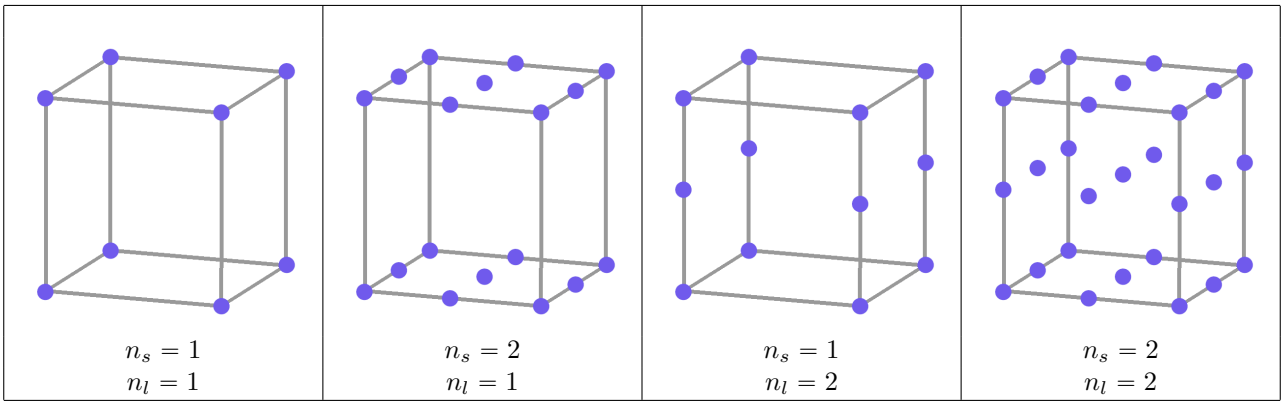

Table 1: Element discretizations across the surface and through the thickness.

4.4. Calculation of the metric tensor and the Christoffel symbols

From the previous construction, we have the covariant basis vectors $\{\boldsymbol{g}_1, \boldsymbol{g}_2, \boldsymbol{g}_3\}$. From equations (4.1) and (4.2) we have these vectors at each point of each element, i.e., we have $\boldsymbol{g}_\alpha|_K(\xi,\eta)$ using isoparametric coordinates, $\alpha = 1,2,3$. In what follows, we will omit the element label and the dependence on (ξ,η) to lighten the notation.

In general, from the covariant basis vectors we may compute at each point the covariant metric tensor $g_{\alpha\beta}$ given by equation (2.2), as well as its contravariant representation $g^{\alpha\beta}$ and, from this, the contravariant basis $\{\boldsymbol{g}^1, \boldsymbol{g}^2, \boldsymbol{g}^3\}$. However, the basis we have constructed are orthonormal, and therefore $g_{\alpha\beta} = g^{\alpha\beta} = \delta_{\alpha\beta}$ and $\boldsymbol{g}^\alpha = \boldsymbol{g}_\alpha$, $\alpha,\beta = 1,2,3$.

It only remains to compute the derivatives with respect to the curvilinear coordinates given by equation (2.5) and, from these, the Christoffel symbols given by equation (2.6). What we may compute from equations (4.1)

and (4.2) are the derivatives of $\{\boldsymbol{g}_1, \boldsymbol{g}_2, \boldsymbol{g}_3\}$ with respect to the isoparametric coordinates (ξ, η) and, if the basis is considered variable with respect to ζ, also with respect to this coordinate. Let us call

$$\nabla_0 \boldsymbol{g}_\alpha = \left(\frac{\partial \boldsymbol{g}_\alpha}{\partial \xi}, \frac{\partial \boldsymbol{g}_\alpha}{\partial \eta}, \frac{\partial \boldsymbol{g}_\alpha}{\partial \zeta} \right), \quad \alpha = 1, 2, 3.$$

Since the curvilinear coordinates $(\theta^1, \theta^2, \theta^3)$ are by construction tangent to $\{\boldsymbol{g}_1, \boldsymbol{g}_2, \boldsymbol{g}_3\}$, we may now compute $\boldsymbol{g}_{\alpha,\beta}$ as the directional derivative

$$\boldsymbol{g}_{\alpha,\beta} \equiv \frac{\partial \boldsymbol{g}_\alpha}{\partial \theta^\beta} = \boldsymbol{g}_\beta \cdot \nabla_0 \boldsymbol{g}_\alpha, \quad \alpha, \beta = 1, 2, 3.$$

From this expression we can compute the Christoffel symbols using equation (2.6). These are needed in the general case. However, we shall see in the next section that we do not need to compute them if the unknowns of the problem are the Cartesian components of the displacement (and the stress in either reference system), despite the equilibrium equations are written in curvilinear coordinates.

This completes the geometrical approximation of the solid-shell.

5. Finite element approximation

5.1. Interpolation of displacements and stresses

The approach we will follow is to use the same interpolation for the displacements as for the geometry, which is also used, for example, in [57]. Therefore, these displacements will be interpolated as

$$\boldsymbol{u}_h(\boldsymbol{x}) = \sum_{a=1}^{n_{\text{pts}}} N^a(\boldsymbol{x}) \hat{u}_i^a \boldsymbol{e}_i \iff \hat{u}_{hi}(\boldsymbol{x}) = \sum_{a=1}^{n_{\text{pts}}} N^a(\boldsymbol{x}) \hat{u}_i^a, \tag{5.1}$$

where $\hat{u}_i^a$ is the i-th Cartesian component of the displacement at node a. Since in the Cartesian basis the covariant and contravariant components coincide, we do not need to distinguish them. Superscripts for the Cartesian components will refer to nodal values from now on.

In the finite element implementation, we shall take *the Cartesian nodal values $\hat{u}_i^a$ as the unknowns of the problem.* Therefore, we need to relate the curvilinear components of the displacement and their derivatives to these nodal values.

According to the transformation rule for displacements in equations (2.19) and (2.11), the covariant components of displacements in curvilinear coordinates can be expressed as

$$u_\alpha = g_{\alpha i} \hat{u}_i = \frac{\partial x_i}{\partial \theta^\alpha} \hat{u}_i, \tag{5.2}$$

at each point, $g_{\alpha i}$ being the i-th component of $\boldsymbol{g}_\alpha$ (not to be confused with the components of the metric tensor). This also follows from $\boldsymbol{u} = u_\beta \boldsymbol{g}^\beta = \hat{u}_i \boldsymbol{e}_i$ and taking the scalar product with $\boldsymbol{g}_\alpha$.

The partial derivative of u_α with respect to θ^β will be

$$\begin{aligned} u_{\alpha,\beta} &= g_{\alpha i} \hat{u}_{i,\beta} + g_{\alpha i,\beta} \hat{u}_i \\ &= g_{\alpha i} g_{\beta j} \hat{u}_{i,j} + g_{\gamma i} \Gamma^\gamma_{\alpha\beta} \hat{u}_i. \end{aligned} \tag{5.3}$$

The chain rule in the form $\hat{u}_{i,\beta} = \hat{u}_{i,j} x^j_{,\beta} = \hat{u}_{i,j} g_{\beta j}$ has been used in the first term and the definition of the Christoffel symbol in the second.

Finally, the covariant derivative of u_α with respect to θ^β will be

$$\begin{aligned} u_{\alpha|\beta} &= u_{\alpha,\beta} - \Gamma^\gamma_{\alpha\beta} u_\gamma \\ &= g_{\alpha i} g_{\beta j} \hat{u}_{i,j} + g_{\gamma i} \Gamma^\gamma_{\alpha\beta} \hat{u}_i - \Gamma^\gamma_{\alpha\beta} g_{\gamma i} \hat{u}_i \\ &= g_{\alpha i} g_{\beta j} \hat{u}_{i,j}. \end{aligned} \tag{5.4}$$

Equations (5.2)-(5.3)-(5.4) are the relationships we need to relate the curvilinear components of the displacement with the Cartesian ones. The latter will be interpolated as indicated in equation (5.1), thus providing the finite

element interpolation for the curvilinear components of the displacement and their derivatives, which will be:

$$\begin{aligned} u_{h\alpha} &= g_{\alpha i}\hat{u}_{hi}, \\ u_{h\alpha,\beta} &= g_{\alpha i}g_{\beta j}\hat{u}_{hi,j} + g_{\gamma i}\Gamma^{\gamma}_{\alpha\beta}\hat{u}_{hi}, \\ u_{h\alpha|\beta} &= g_{\alpha i}g_{\beta j}\hat{u}_{hi,j}. \end{aligned}$$

It is understood that the basis $\{\boldsymbol{g}_1, \boldsymbol{g}_2, \boldsymbol{g}_3\}$ are also constructed from the finite element approximation, as explained in the previous section, although we have not introduced any symbol to distinguish this finite element approximation of the basis functions. It is observed that the Christoffel symbols are not needed to compute the covariant derivates of the covariant components of the displacement. The important expression we shall use is the last one, together with its inverse, which are the discrete counterparts of (2.14) and (2.18):

$$u_{h\alpha|\beta} = g_{\alpha i}g_{\beta j}\hat{u}_{hi,j} = \frac{\partial x_i}{\partial\theta^\alpha}\frac{\partial x_j}{\partial\theta^\beta}\hat{u}_{hi,j} \iff u_{hi,j} = g_i^\alpha g_j^\beta \hat{u}_{h\alpha|\beta} = \frac{\partial\theta^\alpha}{\partial x_i}\frac{\partial\theta^\beta}{\partial x_j}\hat{u}_{h\alpha|\beta}. \tag{5.5}$$

In the case of stresses, they are interpolated in Cartesian coordinates as

$$\boldsymbol{\sigma}_h = \sum_{a=1}^{n_{\text{pts}}} N^a(\boldsymbol{x})\hat{\sigma}^a_{ij}\boldsymbol{e}_i\otimes\boldsymbol{e}_j \iff \hat{\sigma}_{hij} = \sum_{a=1}^{n_{\text{pts}}} N^a(\boldsymbol{x})\hat{\sigma}^a_{ij}, \tag{5.6}$$

where $\hat{\sigma}^a_{ij}$ is the ij-th component of the stress at node a. Now we do not need derivatives of the stresses, but only the expression of their curvilinear components in terms of the Cartesian ones. This can be obtained from equation (2.17), yielding the discrete counterpart of equations (2.13) and (2.17):

$$\sigma_h{}^{\alpha\beta} = g_i^\alpha g_j^\beta \hat{\sigma}_{hij} = \frac{\partial\theta^\alpha}{\partial x_i}\frac{\partial\theta^\beta}{\partial x_j}\hat{\sigma}_{hij} \iff \hat{\sigma}_{hij} = g_{\alpha i}g_{\beta j}\sigma_h{}^{\alpha\beta} = \frac{\partial x_i}{\partial\theta^\alpha}\frac{\partial x_j}{\partial\theta^\beta}\sigma_h{}^{\alpha\beta}. \tag{5.7}$$

Again, let us point out that since the curvilinear coordinate system is orthonormal, the covariant basis coincides with the contravariant one.

5.2. Galerkin finite element approximation

From the partition $\mathcal{T}_h^{3\text{D}} = \{K^{3\text{D}}\}$ of the domain $\Omega^{3\text{D}}$ we can approximate problem (3.6) using finite elements in the standard way. Let $\mathcal{X}_h \subset \mathcal{X}$ be a conforming finite element space, corresponding either to the irreducible or to the mixed form of the problem. The Galerkin approximation consists in finding $\boldsymbol{U}_h \in \mathcal{X}_h$ such that

$$B(\boldsymbol{V}_h, \boldsymbol{U}_h) = L(\boldsymbol{V}_h) \qquad \forall\, \boldsymbol{V}_h \in \mathcal{X}_h. \tag{5.8}$$

In the case of the irreducible formulation, this reads:

$$(\nabla^s\boldsymbol{v}_h, \mathbb{C} : \nabla^s\boldsymbol{u}_h) = \langle \boldsymbol{v}_h, \rho\boldsymbol{b}\rangle. \tag{5.9}$$

This equation and the following are *intrinsic*, i.e., they do not depend on the coordinate system. In the following subsection we will consider the particular cases of Cartesian and curvilinear coordinates.

The standard stability estimate for the irreducible formulation can be obtained simply by taking $\boldsymbol{v}_h = \boldsymbol{u}_h$ in equation (5.9), yielding

$$(\nabla^s\boldsymbol{u}_h, \mathbb{C} : \nabla^s\boldsymbol{u}_h) = \|\boldsymbol{u}_h\|_E^2 \lesssim \|\boldsymbol{u}_h\|_E\|\rho\boldsymbol{b}\|_{E'} \tag{5.10}$$

where $\|\cdot\|_E$ is the energy norm, $\|\cdot\|_{E'}$ its dual and $\lesssim$ stands for $\leqslant$ up to positive constants. In this case, $\|\boldsymbol{u}_h\|_E$ corresponds to the discrete internal elastic energy (up to constants). The result $\|\boldsymbol{u}_h\|_E \lesssim \|\rho\boldsymbol{b}\|_{E'}$ implies that the irreducible formulation is numerically stable if the tensor $\mathbb{C}$ is positive definite. However, being numerically stable does not guarantee the approximation to be free of numerical locking. In fact, membrane and shear locking are anticipated when using standard low order 3D elements for the approximation of thin structures.

On the other hand, the Galerkin form in equation (5.8) for the mixed formulation reads:

$$(\nabla^s\boldsymbol{v}_h, \boldsymbol{\sigma}_h) = \langle \boldsymbol{v}_h, \rho\boldsymbol{b}\rangle, \tag{5.11}$$

$$-(\boldsymbol{\tau}_h, \mathbb{C}^{-1} : \boldsymbol{\sigma}_h) + (\boldsymbol{\tau}_h, \nabla^s\boldsymbol{u}_h) = \boldsymbol{0}. \tag{5.12}$$

The standard Galerkin approach to this formulation using continuous interpolations for both displacements and stress fields is not stable. The stability depends on the compatibility restrictions on the finite element spaces for the displacements $\mathcal{U}_h \subset \mathcal{U}$ and for the stresses $\mathcal{S}_h \subset \mathcal{S}$ chosen, which have to fulfil the inf-sup condition. The instability due to not satisfying this condition pollutes the solution in the form of uncontrollable oscillations in the displacement field. The reader can refer to [75] for a detailed explanation regarding these conditions.

5.3. Stabilized finite element approximation

The idea of stabilized finite element methods is to overcome the instability of the Galerkin approach by modifying the variational form of the problem through the introduction of consistent terms that allow one to obtain stable solutions independently of the choice of the interpolation spaces. The stabilization employed in the present work is based on the VMS approach [65, 66, 67]. This approach has been previously discussed in [76] for the linear elastic solid problem and in [77] for solid-shell elements using Cartesian coordinates, and it is explored further in the present work by taking advantage of the local curvilinear basis which define the tangent and normal components of the stresses.

The idea of the VMS stabilization employed in this paper consists of adding additional terms to the Galerkin formulation, that enhance stability without upsetting accuracy. It starts by splitting the space of unknowns as $\mathcal{X} = \mathcal{X}_h \oplus \mathcal{X}'$, where $\mathcal{X}_h$ is the component that can be resolved in the finite element space and $\mathcal{X}'$ is the remainder, called sub-grid scale (SGS) space. In this manner, the unknowns are split as $\boldsymbol{U} = \boldsymbol{U}_h + \boldsymbol{U}'$, and also the test functions as $\boldsymbol{V} = \boldsymbol{V}_h + \boldsymbol{V}'$. The splitting modifies the original formulation (5.8) and the problem consists of finding $\boldsymbol{U}_h \in \mathcal{X}_h$ and $\boldsymbol{U}' \in \mathcal{X}'$ such that

$$B\left(\boldsymbol{V}_h, \boldsymbol{U}_h\right) + B\left(\boldsymbol{V}_h, \boldsymbol{U}'\right) = L\left(\boldsymbol{V}_h\right) \qquad \forall\, \boldsymbol{V}_h \in \mathcal{X}_h, \tag{5.13}$$

$$B\left(\boldsymbol{V}', \boldsymbol{U}_h\right) + B\left(\boldsymbol{V}', \boldsymbol{U}'\right) = L\left(\boldsymbol{V}'\right) \qquad \forall\, \boldsymbol{V}' \in \mathcal{X}', \tag{5.14}$$

where (5.13) is the finite element equation and (5.14) is the SGS equation. Note that choosing $\mathcal{X}' = \{0\}$ yields the Galerkin method, making the stabilization to be consistent by construction. Incorporating the SGSs in equation (5.13) modifies the original problem in equations (5.11)-(5.12) as follows:

$$(\nabla^s \boldsymbol{v}_h, \boldsymbol{\sigma}_h) + (\nabla^s \boldsymbol{v}_h, \boldsymbol{\sigma}') = \langle \boldsymbol{v}_h, \rho \boldsymbol{b} \rangle, \tag{5.15}$$

$$-(\boldsymbol{\tau}_h, \mathbb{C}^{-1} : \boldsymbol{\sigma}_h) + (\boldsymbol{\tau}_h, \nabla^s \boldsymbol{u}_h) - (\boldsymbol{\tau}_h, \mathbb{C}^{-1} : \boldsymbol{\sigma}') + (\boldsymbol{\tau}_h, \nabla^s \boldsymbol{u}') = \boldsymbol{0}. \tag{5.16}$$

Under this framework, it only remains to find an approximation of the SGSs. The objective is to express these SGSs in terms of the finite element variables, thus preserving the initial number of unknowns of the problem. The approximation needed can be achieved by working on equation (5.14), noting that

$$\begin{aligned} B\left(\boldsymbol{V}', \boldsymbol{U}'\right) &= L\left(\boldsymbol{V}'\right) - B\left(\boldsymbol{V}', \boldsymbol{U}_h\right), \\ &= L\left(\boldsymbol{V}'\right) - \sum_K \left\langle \boldsymbol{V}', \mathcal{L}\boldsymbol{U}_h \right\rangle_K, \\ &= \sum_K \left\langle \boldsymbol{V}', \mathcal{R}\boldsymbol{U}_h \right\rangle_K, \end{aligned} \tag{5.17}$$

where $\langle \cdot, \cdot \rangle_K$ is the integral of the product of two functions over an element domain K and $\mathcal{R}\boldsymbol{U}_h = \boldsymbol{F} - \mathcal{L}\boldsymbol{U}_h$ is the finite element residual, defined as

$$\mathcal{R}\boldsymbol{U}_h = \begin{bmatrix} \mathcal{R}_u \boldsymbol{U}_h \\ \mathcal{R}_\sigma \boldsymbol{U}_h \end{bmatrix} = \begin{bmatrix} \rho \boldsymbol{b} + \nabla \cdot \boldsymbol{\sigma}_h \\ \mathbb{C}^{-1} : \boldsymbol{\sigma}_h - \nabla^s \boldsymbol{u}_h \end{bmatrix}.$$

In the second step to obtain equation (5.17) it has been considered that the SGSs vanish on the element boundaries. This approximation will also be used in the following, although it can be relaxed as explained in [78].

The specific details of how to obtain the SGSs can be reviewed in [79]. After some mathematical approximations, the SGSs $\boldsymbol{U}' = [\boldsymbol{u}', \boldsymbol{\sigma}']^T$ can then be taken as

$$\boldsymbol{U}' \,|_K \approx \boldsymbol{\tau}_K P'\left(\mathcal{R}\boldsymbol{U}_h\right)|_K, \tag{5.18}$$

where P' is the L^2 projection onto the SGS space $\mathcal{X}'$ and the matrix of stabilization parameters $\boldsymbol{\tau}_K$, which approx-

imates $\mathcal{L}^{-1}$ on each element K, is computed as

$$\boldsymbol{\tau}_K = \begin{bmatrix} \tau_u \boldsymbol{I}_3 & \mathbf{0} \\ \mathbf{0} & \tau_\sigma \boldsymbol{I}_6 \end{bmatrix}, \qquad \tau_u = c_u \frac{h}{L_0}, \qquad \tau_\sigma = c_\sigma \frac{L_0 h}{C_{\min}},$$

where $\boldsymbol{I}_3$ and $\boldsymbol{I}_6$ are the identity on vectors and on symmetric second order tensors, respectively, c_u and c_σ are algorithmic constants, L_0 is a characteristic length of the domain, h is the element size, and $C_{\min}$ is the smallest eigenvalue of $\mathbb{C}$. As it is explained in [76], the calculation of the stabilization parameters proposed is the one that provides optimal accuracy when equal interpolation is used for the stresses and the displacements.

The SGS can then be incorporated into (5.13) by taking advantage of the additivity of the integral and the fact that, assuming $\boldsymbol{U}' = \mathbf{0}$ on the interelement boundaries:

$$B\left(\boldsymbol{V}, \boldsymbol{U}'\right) = \sum_K \left\langle \boldsymbol{V}, \mathcal{L}\boldsymbol{U}' \right\rangle_K = \sum_K \left\langle \mathcal{L}^* \boldsymbol{V}, \boldsymbol{U}' \right\rangle_K, \tag{5.19}$$

where the superscript * denotes the adjoint of an operator, which comes from the integration by parts of the original operator. In this manner, using the expression for the SGSs in equation (5.18) and the property (5.19) into equation (5.13) yields the stabilized formulation

$$B\left(\boldsymbol{V}_h, \boldsymbol{U}_h\right) + \sum_K \left\langle \mathcal{L}^* \boldsymbol{V}_h, \boldsymbol{\tau}_K P'\left(\mathcal{R}\boldsymbol{U}_h\right) \right\rangle_K = L(\boldsymbol{V}_h). \tag{5.20}$$

It only remains to choose the space of the SGS, and thus how the projection P' is approximated.

A typical choice of the SGS space is taking it as the space of finite element residuals, leading to the Algebraic Subgrid Scale (ASGS) formulation. In this case, $P' = I$, resulting in

$$\boldsymbol{u}' = \tau_u(\rho \boldsymbol{b} + \nabla \cdot \boldsymbol{\sigma}_h), \quad \boldsymbol{\sigma}' = \tau_\sigma \left(\mathbb{C} : \nabla^s \boldsymbol{u}_h\right).$$

However, in this work, the SGS space is considered to be the L^2 orthogonal to the finite element space, so that $\mathcal{X} = \mathcal{X}_h \oplus \mathcal{X}_h^\perp$. Following this approach yields the Orthogonal Subgrid Scale (OSGS) formulation, in which $P' = P_h^\perp = I - P_h$, P_h being the L^2 projection onto $\mathcal{X}_h$. Therefore, the SGSs $\boldsymbol{U}'$ defined in (5.18) are computed as

$$\boldsymbol{u}' = \tau_u P_h^\perp(\rho \boldsymbol{b} + \nabla \cdot \boldsymbol{\sigma}_h) = \tau_u \left[\rho \boldsymbol{b} + \nabla \cdot \boldsymbol{\sigma}_h - P_h(\rho \boldsymbol{b} + \nabla \cdot \boldsymbol{\sigma}_h)\right], \tag{5.21}$$

$$\boldsymbol{\sigma}' = \tau_\sigma P_h^\perp \left(\mathbb{C} : \nabla^s \boldsymbol{u}_h\right) \quad = \tau_\sigma \left[\mathbb{C} : \nabla^s \boldsymbol{u}_h - P_h \left(\mathbb{C} : \nabla^s \boldsymbol{u}_h\right)\right], \tag{5.22}$$

where the term corresponding to $P_h^\perp(\boldsymbol{\sigma}_h)$ vanishes because $\boldsymbol{\sigma}_h$ is in the finite element space and it is being projected onto its orthogonal counterpart.

Using the SGSs given in (5.21)-(5.22) in equations (5.15)-(5.16) yields

$$(\nabla^s \boldsymbol{v}_h, \boldsymbol{\sigma}_h) + \tau_\sigma(\nabla^s \boldsymbol{v}_h, \mathbb{C} : \nabla^s \boldsymbol{u}_h - P_h(\mathbb{C} : \nabla^s \boldsymbol{u}_h)) = (\boldsymbol{v}_h, \rho \boldsymbol{b}), \tag{5.23}$$

$$-(\boldsymbol{\tau}_h, \mathbb{C}^{-1} : \boldsymbol{\sigma}_h) + (\boldsymbol{\tau}_h, \nabla^s \boldsymbol{u}_h) - \tau_u(\nabla \cdot \boldsymbol{\tau}_h, \nabla \cdot \boldsymbol{\sigma}_h - P_h(\nabla \cdot \boldsymbol{\sigma}_h)) = \tau_u(\nabla \cdot \boldsymbol{\tau}_h, \rho \boldsymbol{b} - P_h(\rho \boldsymbol{b})), \tag{5.24}$$

where the term $\tau_\sigma(\boldsymbol{\tau}_h, \mathbb{C}^{-1} : \boldsymbol{\sigma}')$ vanishes due to the orthogonality condition (assuming constant physical properties).

5.4. Finite element formulations in Cartesian and curvilinear coordinates

The equations that need to be solved are equation (5.9) in the irreducible formulation and equations (5.23)-(5.24) in the case of the mixed stabilized formulation. The former is expected to yield locking in the case of thin structures, and it is irrelevant whether it is solved in Cartesian or curvilinear coordinates, as the degrees of freedom are the three displacement components in either system of coordinates. We shall solve them in Cartesian coordinates, i.e., we will solve the problem of finding $\hat{\boldsymbol{u}}_h \in \mathcal{U}_h$ such that

$$(\hat{v}_{hi,j}, \hat{\mathbb{C}}_{ijkl} \hat{u}_{hk,l}) = \langle \hat{v}_{hi}, \rho \hat{b}_i \rangle \qquad \forall \hat{\boldsymbol{v}}_h \in \mathcal{U}_h. \tag{5.25}$$

To simplify the writing, we have used the whole displacement gradient instead of its symmetric part; the contraction with the constitutive tensor, satisfying the major and minor symmetries, will produce the same result. Note also that we have considered homogeneous boundary conditions for displacements on the whole boundary; non-homogeneous displacements on part of the boundary and normal stresses on the complement could be easily acomodated.

Even if we will not used it, equation (5.25) can be transformed to curvilinear coordinates using expression (5.5) as

$$\left(\frac{\partial\theta^\alpha}{\partial x_i}\frac{\partial\theta^\beta}{\partial x_j}v_{h\alpha|\beta},\hat{\mathbb{C}}_{ijkl}\frac{\partial\theta^\gamma}{\partial x_k}\frac{\partial\theta^\delta}{\partial x_l}u_{h\gamma|\delta}\right)=\langle v_{h\alpha},\rho b^\alpha\rangle. \tag{5.26}$$

Let us move now to the mixed stabilized formulation. In our numerical experience, we have found that the parameter τ_u can often be set to $\tau_u=0$ and still have a stable and accurate approximation. To simplify the writing, let us consider that this is the case. Problem (5.23)-(5.24) in Cartesian coordinates consists of finding $[\hat{\boldsymbol{u}}_h,\hat{\boldsymbol{\sigma}}_h]\in\mathcal{X}_h$ such that

$$(\hat{v}_{hi,j},\hat{\sigma}_{hij})+\tau_\sigma(\hat{v}_{hi,j},\hat{\mathbb{C}}_{ijkl}\hat{u}_{hk,l}-P_h(\hat{\mathbb{C}}_{ijkl}\hat{u}_{hk,l}))=\langle\hat{v}_{hi},\rho\hat{b}_i\rangle\qquad\forall\hat{\boldsymbol{v}}_h\in\mathcal{U}_h, \tag{5.27}$$

$$-(\hat{\tau}_{hij},\hat{\mathbb{C}}^{-1}_{ijkl}\hat{\sigma}_{hkl})+(\hat{\tau}_{hij},\hat{u}_{hi,j})=0\qquad\forall\hat{\boldsymbol{\tau}}_h\in\mathcal{S}_h. \tag{5.28}$$

Recall that we are imposing strongly the symmetry of the stresses and the stress test functions.

We can now write problem (5.27)-(5.28) in curvilinear coordinates using the transformation rules (5.5)-(5.7), yielding:

$$\begin{aligned}\left(v_{h\alpha|\beta},\sigma_h^{\alpha\beta}\right)+\tau_\sigma\left(\frac{\partial\theta^\alpha}{\partial x_i}\frac{\partial\theta^\beta}{\partial x_j}v_{h\alpha|\beta},\hat{\mathbb{C}}_{ijkl}\frac{\partial\theta^\gamma}{\partial x_k}\frac{\partial\theta^\delta}{\partial x_l}u_{h\gamma|\delta}-P_h\Big[\hat{\mathbb{C}}_{ijkl}\frac{\partial\theta^\gamma}{\partial x_k}\frac{\partial\theta^\delta}{\partial x_l}u_{h\gamma|\delta}\Big]\right)&=\langle v_{h\alpha},\rho b^\alpha\rangle,\\ -\left(\frac{\partial x_i}{\partial\theta^\alpha}\frac{\partial x_j}{\partial\theta^\beta}\tau_h^{\alpha\beta},\hat{\mathbb{C}}^{-1}_{ijkl}\frac{\partial x_k}{\partial\theta^\gamma}\frac{\partial x_l}{\partial\theta^\delta}\sigma_h^{\gamma\delta}\right)+\left(\tau_h^{\alpha\beta},u_{h\alpha|\beta}\right)&=0.\end{aligned}$$

Finally, we can consider a *hybrid* approach, using displacements in Cartesian coordinates and stresses in curvilinear coordinates. The convenience of this approach will be clear in the following subsection. Using again the transformation rules (5.5)-(5.7), we obtain:

$$\left(\hat{v}_{hi,j},\frac{\partial x_i}{\partial\theta^\alpha}\frac{\partial x_j}{\partial\theta^\beta}\sigma_h^{\alpha\beta}\right)+\tau_\sigma\left(\hat{v}_{hi,j},\hat{\mathbb{C}}_{ijkl}\hat{u}_{hk,l}-P_h(\hat{\mathbb{C}}_{ijkl}\hat{u}_{hk,l})\right)=\langle\hat{v}_i^h,\rho\hat{b}_i\rangle, \tag{5.29}$$

$$-\left(\frac{\partial x_i}{\partial\theta^\alpha}\frac{\partial x_j}{\partial\theta^\beta}\tau_h^{\alpha\beta},\hat{\mathbb{C}}^{-1}_{ijkl}\frac{\partial x_k}{\partial\theta^\gamma}\frac{\partial x_l}{\partial\theta^\delta}\sigma_h^{\gamma\delta}\right)+\left(\frac{\partial x_i}{\partial\theta^\alpha}\frac{\partial x_j}{\partial\theta^\beta}\tau_h^{\alpha\beta},u_{hi,j}\right)=0. \tag{5.30}$$

Let us point out that at the continuous level $\frac{\partial x_i}{\partial\theta^\alpha}=g_{\alpha i}$, but in fact vectors $\boldsymbol{g}_\alpha$, $\alpha=1,2,3$, are computed as described in subsection 4.1.

5.5. Deactivation of stress degrees of freedom

The convenience of equations (5.29)-(5.30) relies on the fact that, on the one hand, displacements are approximated in Cartesian coordinates, easier to handle than the curvilinear ones, and on the other hand stresses are expressed in curvilinear coordinates, thus having a mechanical meaning. In these equations, *all* the stress components are considered independent variables. However, to study which stresses need to be interpolated independently to avoid locking, we may consider a switch between their independent interpolation and their expression in terms of the (Cartesian) displacements. This switch can be constructed by redefining the stresses as

$$\sigma_h^{\alpha\beta}\leftarrow\chi^{\alpha\beta}\sigma_h^{\alpha\beta}+(1-\chi^{\alpha\beta})\frac{\partial\theta^\alpha}{\partial x_i}\frac{\partial\theta^\beta}{\partial x_j}\hat{\mathbb{C}}_{ijkl}\hat{u}_{hk,l}\quad(\text{no sum on }\alpha,\beta), \tag{5.31}$$

where $\chi^{\alpha\beta}=1$ indicates that the stress $\sigma_h^{\alpha\beta}$ is an independent unknown, whereas if $\chi^{\alpha\beta}=0$ this stress is computed in terms of the displacement, and likewise for the stress test function. In this last case, the corresponding equation $\alpha\beta$ in (5.30) is simply deleted. Note that if $\chi^{\alpha\beta}=0$ for all α and β, equation (5.29) with $\tau_\sigma=0$ reduces to equation (5.25) and equation (5.30) becomes $0=0$.

Equation (5.31) provides a mechanism for activating or deactivating the stress components as independent variables that will be explored in the numerical examples presented next.

6. Numerical results

It is known that all types of numerical locking appear in solid-shell elements when specific conditions are met. This issue has been proven to be solved by using the stabilized mixed formulation of the VMS type [77]. In this context, numerical locking is solved by using a mixed formulation where the stresses are interpolated as unknowns

and are stabilized to circumvent the inf-sup condition. The shear locking problems are solved because the zero shear strain condition can be properly represented by the shear stresses. On the other hand, membrane locking is solved by obtaining control over the parasitic strains by formulating properly scaled membrane strains. Similarly, trapezoidal locking is solved by eliminating the parasitic transverse normal strains by formulating a properly scaled strain in that direction. However, identifying when is it convenient to interpolate each component of the stress tensor remains to be examined in depth. Reducing the number of unknowns to be solved can be fruitful to optimize the computational resources. To properly examine this possibility, the logical step is to set a list of benchmark problems and solve them interpolating as unknowns only part of the stress tensor. In this manner, the influence of each of the stresses can be described independently, and the combinations that can maintain the accuracy of the solution can be found. In the context of plate and shell structures, the stresses can be classified into four groups depending on the direction they act: membrane stresses, transverse stress, twisting stresses, and shear stresses (see Fig. 1). Therefore the stresses are chosen considering this grouping instead of independently. Let us stress again that curvilinear coordinates are needed in the case of shells to classify the stresses.

In the following, some benchmark cases are solved to describe the numerical response of thin structures with respect to the irreducible and mixed formulations. The initial cases are flat plate benchmark problems, serving as a starting point due to their simplicity. Afterward, shell benchmark problems are solved considering the inherent complexity of curved structures. The importance of shell cases lies in the variety of mechanical responses they present when subject to different types of loads and boundary conditions. Additionally, the study takes into account the order of interpolation across the shell surface n_s and through the thickness n_l, as well as the number of elements used in the thickness direction n_{elem}, which has proven to be an important factor in the solid-shell context when dealing with Poisson thickness locking [80].

The physical parameters used are taken from the references. Often, some unphysical values are used and also unphysical results are obtained. Nevertheless, we prefer to keep these values to compare our results with those published in the literature. No unit system is specified, understanding that all units used are consistent.

6.1. Analysis of plates

In this section, the performance of the stabilized mixed and the irreducible formulations presented in sections 5.2-5.3 are compared in two plate benchmark cases. The first case is the clamped circular plate under a uniformly distributed transverse load. Due to the symmetry of the geometry and the applied load, this case reduces to a one-dimensional problem, making it one of the simplest possible cases to be solved. The problem is designed in the classical manner found in the literature [81, 32, 82], by only modeling a quarter of the plate and dividing the domain into three patches with a structured mesh of bilinear elements in each, as described in Fig. 4. The radius of the plate is $R = 5$ and the thickness is $t = 0.1$, resulting in a slenderness ratio of $2R/t = 100$. The load is set to $q = -1$ per unit of surface across the entire surface. The material properties are $E = 10.92$ for Young's modulus and $\nu = 0.3$ for the Poisson number. The results are tracked at the center of the plate where the maximum deflection is 9778.1.

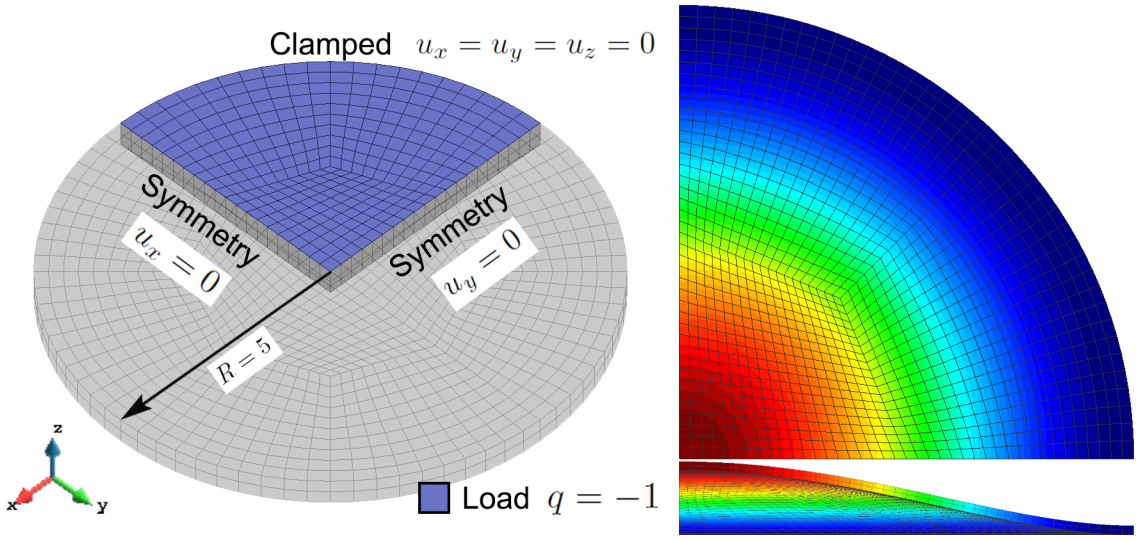

Figure 4: Clamped circular plate: geometry and boundary conditions (left) and deformed configuration (right).

The second case is the clamped square plate under uniform distributed transverse load, a classical benchmark problem found in the literature [81]. This case is similar to the previous one; however, it does not reduce to a one-dimensional problem. Due to symmetry, only a quarter of the plate is modeled. Geometry and boundary conditions are shown in Fig. 5. The square has sides of length $L = 2$ and the thickness is $t = 0.01$, which yields a slenderness ratio of $L/t = 200$. The load is set to $q = -1$ per unit of surface, across the entire surface. The material properties are $E = 17.472 \cdot 10^6$ for Young's modulus and $\nu = 0.3$ for the Poisson number. Results are tracked at the center of the plate where the maximum deflection is 1.26.

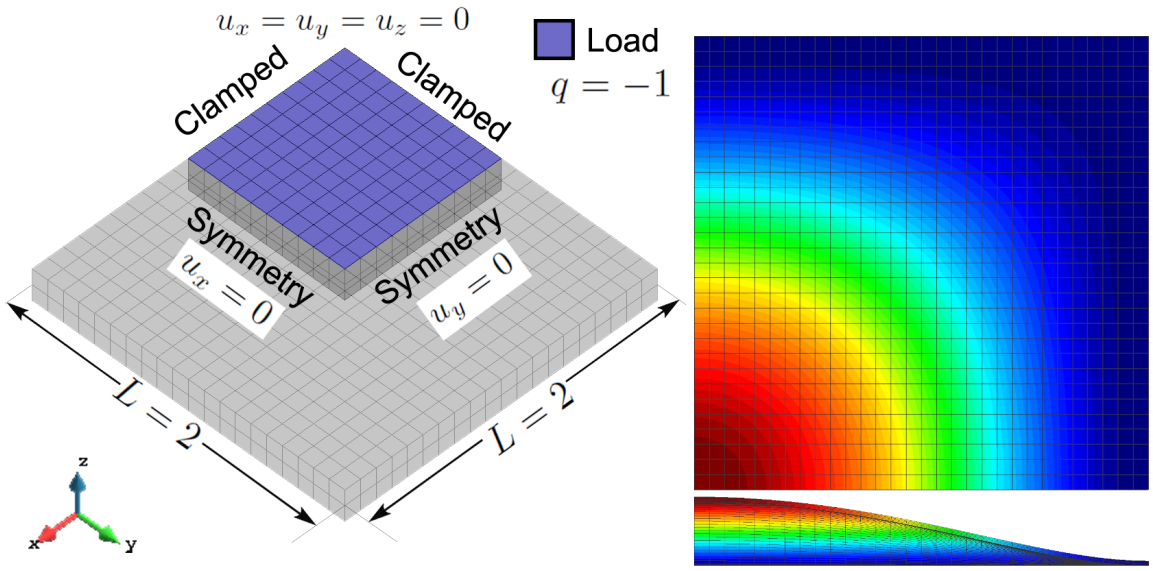

Figure 5: Clamped square plate: geometry and boundary conditions (left) and deformed configuration (right).

Computations are first performed using the irreducible formulation to evaluate its capability to represent the bending state concerning numerical locking. Results for the circular and square plates are plotted in Fig. 6, solved using different combinations of n_s, n_l, and n_{elem}. As usual, relative displacement refers to the quotient between the reference solution and the solution we have computed. The membrane and shear locking behavior is present in the cases of linear interpolation across the surface and they seem to disappear when the order is increased to quadratic. On the other hand, thickness locking is present when computed using linear through-the-thickness interpolation; therefore, a better description of the thickness strain is required. Using more linear elements in the transverse direction seems to slowly mitigate the locking behavior, but it can be solved immediately by using quadratic interpolation even with a single thickness element.

This misbehavior is examined further, considering that increasing the order of interpolation in the thickness direction allows for proper convergence. Fig. 7 shows convergence curves of cases using quadratic interpolation across the surface and up to 6 linear elements in the thickness direction. Results show that by adding more elements in the transverse direction yields little improvement in convergence. It becomes more clear that using a quadratic interpolation in the transverse direction yields better convergence and uses fewer resources compared to the option of adding more elements. These tests are useful to prove that capturing the through-the-thickness behavior is essential to have a proper approximation of the physical problem.

The same cases are solved using the stabilized mixed formulation. The interpolation order across the surface is set to $n_s = 1$, because the stabilized formulation deals with parasitic strains even when using linear elements. Therefore it should be free of membrane, shear and trapezoidal locking effects. The discretization through the thickness consists of $n_{\text{elem}} = \{1, 2\}$ elements, and interpolation orders of $n_l = \{1, 2\}$. Results are plotted in Fig. 8. The stabilized formulation is effective in dealing with numerical locking, except for the thickness locking. Unlike the second order irreducible approximation that needs quadratic transverse interpolation, thickness locking can be solved by using the stabilized formulation and either two elements or set quadratic interpolation through the thickness.

The mechanical response of the plate problems are now checked using the mixed formulation and deactivating some of the stress degrees of freedom. However, it is tested considering that using a single linear through-the-thickness element yields thickness locking solutions. Therefore, computations are focused on either two elements or quadratic interpolations. Results are shown in Figs. 9-10, where they are compared to the full mixed formulation,

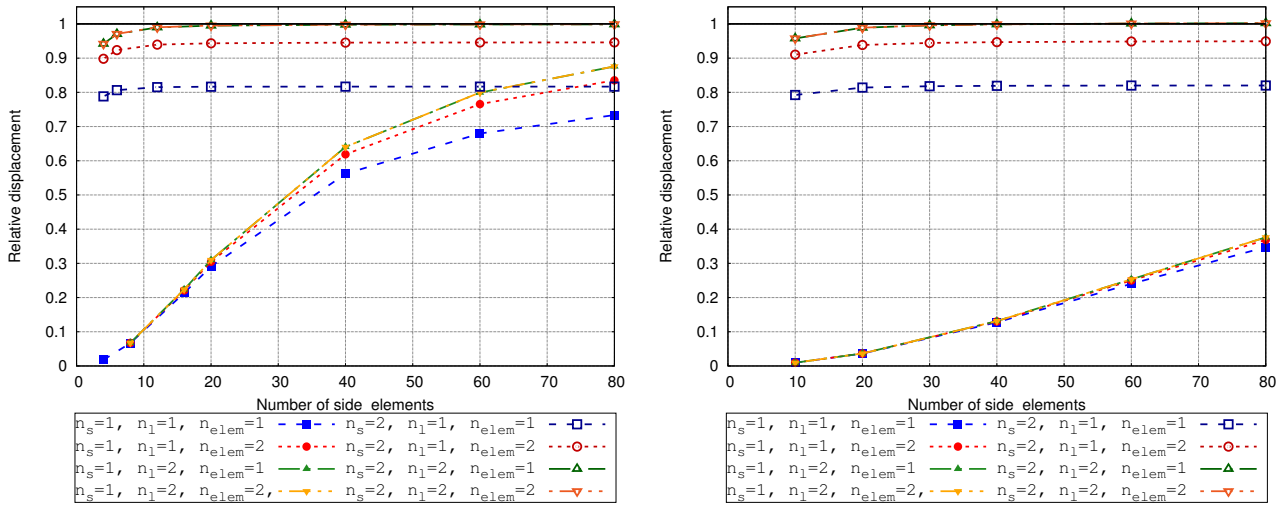

Figure 6: Irreducible formulation convergence for 1 and 2 elements through the thickness using linear and quadratic interpolations: circular plate (left) and square plate (right).

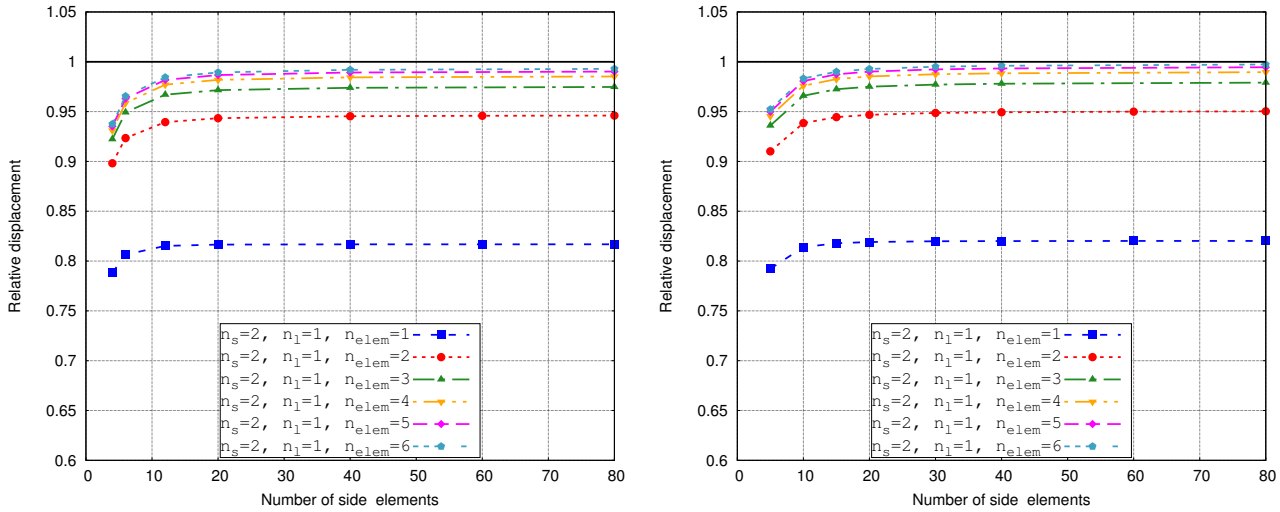

Figure 7: Irreducible formulation convergence curves for increasing number of linear elements through the thickness: circular plate (left) and square plate (right).

and to the irreducible formulation with quadratic interpolation across the surface to avoid shear and membrane locking.

Results confirm that the shear stress group fulfils the role of solving the shear locking in the case of plates. This result is expected and agrees with the Reissner-Mindlin plate theory, which is handled by controlling the shear strain terms [82]. Apart of the shear stress group, all other stress groups should not be necessary. However, when deactivating the thickness stress σ_z in the $n_{\text{nelem}} = 2$ approximation, it becomes clear that it is affected by thickness locking, not as in the case of $n_l = 2$. Therefore, the stabilization in the thickness direction must be activated to be effective in dealing with thickness locking. It has been confirmed that in the case of plates, the shear and thickness stresses are the only groups that matter to obtain locking-free solutions. Consequently, the total number of degrees of freedom can be reduced from 9 to 6 per node if using $n_{\text{nelem}} = 2$ (three displacements, two shear stresses and the transverse stress) or from 9 to 5 if using $n_l = 2$ (three displacements and two shear stresses). This is valid for plate structures, which do not suffer membrane or trapezoidal locking. To have a better understanding of the general behavior of thin structures, it is necessary to move from flat plates to curved shells.

6.2. Analysis of shells

To evaluate the mechanical response of shells it is necessary to consider curved structures, as well as specific loads that make the problem to be membrane or bending dominated. This section presents the mechanical analysis

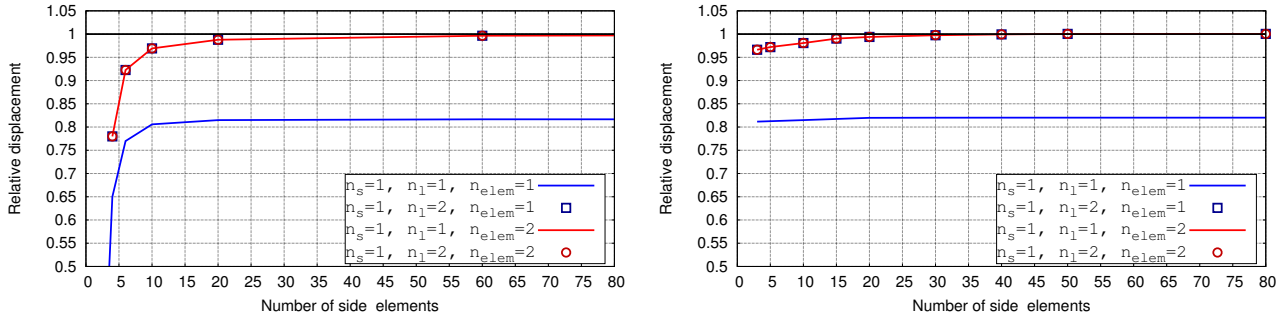

Figure 8: Stabilized formulation convergence: circular plate (left) and square plate (right).

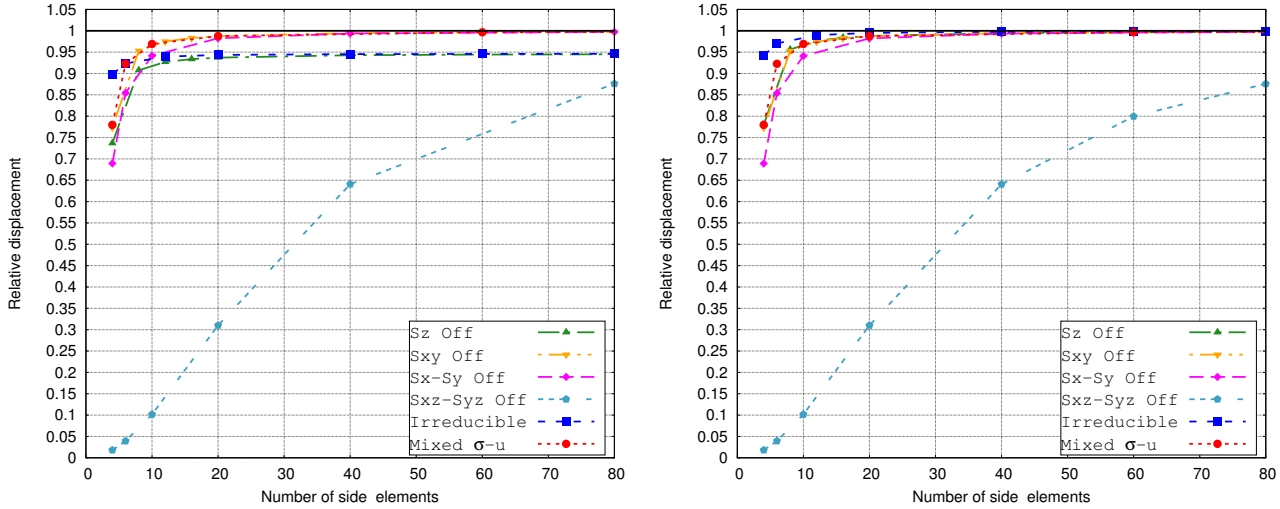

Figure 9: Circular plate: Stress deactivation convergence curves using $n_{\text{nelem}} = 2$ (left) and $n_l = 2$ (right).

of shell structures using the irreducible and the stabilized mixed formulation. It has been proved in subsection 6.1 that thickness locking can be avoided either by increasing the order of interpolation or by increasing the number of elements in the thickness direction.

In the case of plates, it has also been shown in subsection 6.1 that the irreducible formulation suffers numerical locking when using linear interpolations across the surface and thickness directions. Because of that, computations are mainly performed using full quadratic interpolations. Nevertheless, some approximations are computed using a single linear element through the thickness to illustrate the effects of thickness locking effects.

Shell elements are usually tested using a set of tests specifically designed to evaluate the capabilities of elements to have a good performance. The tests considered in this work are taken from the literature [83, 84], and consist in subjecting shells to either inextensional bending, membrane stresses or rigid body motions. The most commonly used tests are the following:

- The Scordelis-Lo roof and the twisted beam problems are designed to evaluate the capabilities to solve membrane strain states, whereas inextensional bending is not relevant.
- The hemispherical shell problem is used to evaluate inextensional bending modes with little membrane strain and also check if the element can reproduce rigid body rotations with respect to the shell surface normals.
- The pinched cylinder problem is a test that subjects the element to a high degree of inextensional bending modes as well as membrane strains.

In the examples below, the performance of the stabilized mixed formulation is compared with respect to the irreducible formulation. The tests are performed using different values of n_s, n_l and n_{elem} for the interpolations. Subsequently, the same tests are performed for the mixed formulation while deactivating the membrane, shear, twisting, and thickness stresses. In that manner, the role of each one of the stresses in the stabilized formulation is put to test, and the implications of loading types and boundary conditions of each case are evaluated.

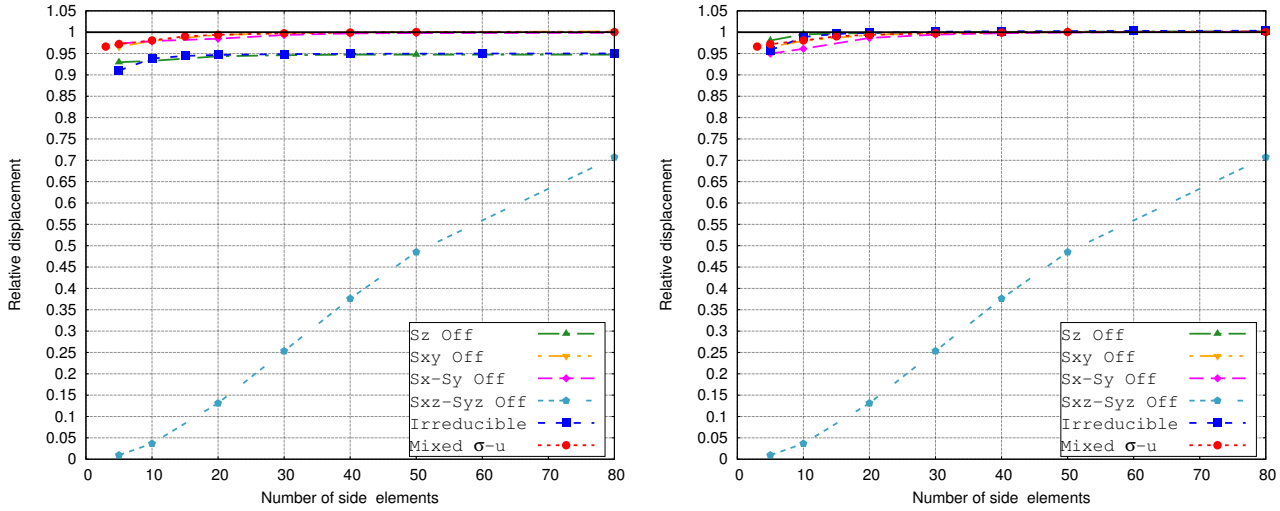

Figure 10: Square plate: Stress deactivation convergence curves using $n_{\text{nelem}} = 2$ (left) and $n_l = 2$ (right).

6.2.1. Scordelis-Lo roof

The problem consists of a single curvature cylindrical panel supported by rigid diaphragms at both ends and loaded vertically. Due to the symmetry of the problem, only a quarter of the shell is modeled using proper symmetry boundary conditions. The length of the roof is $L = 50$, the radius is $R = 25$, and the thickness is $t = 0.25$, which correspond to a slenderness ratio of $L/t = 200$. The loading is set to $q = -90$ per unit of surface across the upper surface. The geometry and boundary conditions are illustrated in Fig. 11. The material properties are $E = 4.32 \cdot 10^8$ for Young's modulus and $\nu = 0$ for Poisson's ratio. The solution is tracked at the mid side of the free edge, whose vertical displacement is between 0.3024 and 0.3086 according to the different authors [77, 85, 86]; however, in the present work the reference displacement is taken to be 0.3037.

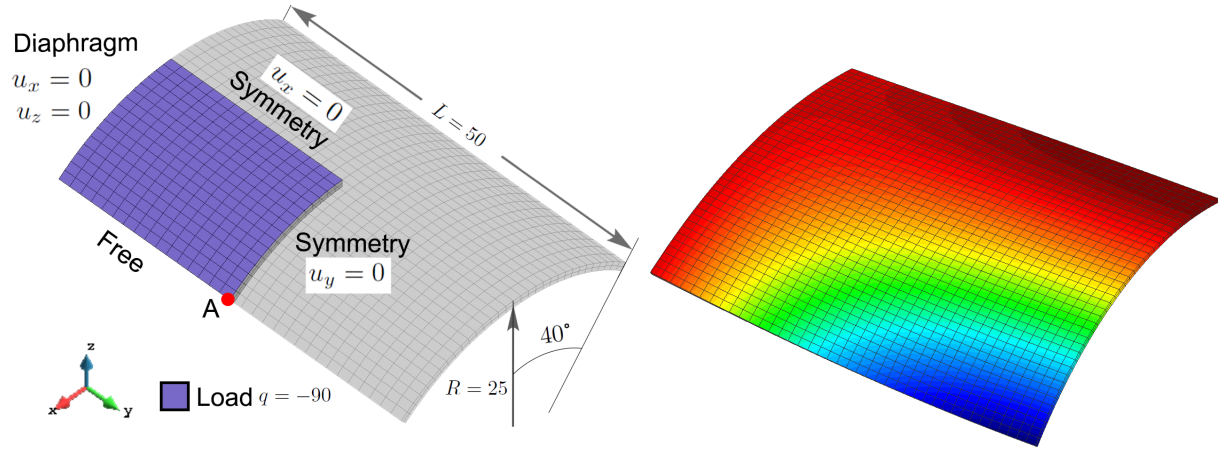

Figure 11: Scordelis-Lo roof: geometry and boundary conditions (left) and deformed configuration (right).

Results for the irreducible and the mixed formulation are shown in Fig. 12, where convergence ratios of the relative displacements with respect to the number of elements are plotted. Compared to flat plate examples, which are affected only by shear and thickness locking, the present example is a curved structure and is affected by membrane and trapezoidal locking. As expected, using quadratic interpolation across the surface yields locking-free results. However, unlike the results found in the plate examples of subsection 6.1, this case does not present thickness locking due to the fact that it depends only on Poisson's ratio. This proves to be a good example to check that thickness locking does not depend on the formulation or the through-the-thickness interpolation choice, and since $\nu = 0$, it is natural that thickness locking disappears. Still, results prove that curvature adds an important difficulty for the problem to be solved properly.

Let us now deactivate strain groups in the mixed formulation and plot convergence curves as shown in Fig. 13.

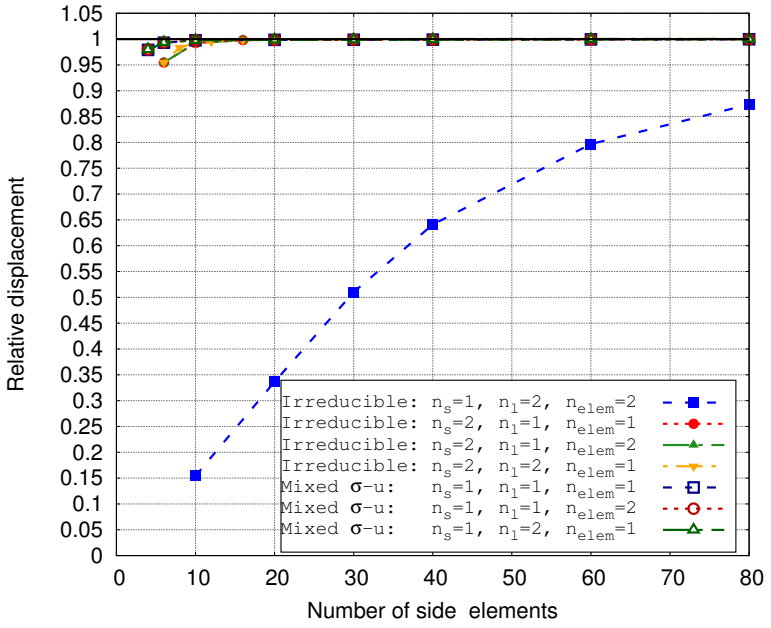

Figure 12: Scordelis-Lo roof: convergence curves using irreducible and mixed formulations.

The notation used in this and subsequent figures is as follows: S_z stands for the thickness stress, S_{xy} for the twisting stress, S_x and S_y for the membrane stresses and S_{xz} and S_{yz} for the membrane stresses, even if these stress components correspond to the local basis and not to the Cartesian one. In this case, shear stresses are needed to overcome shear locking, while normal thickness stress is necessary to overcome trapezoidal locking. Curiously, even though the Scordelis-Lo roof is a case to test membrane strain states, deactivating membrane stresses has no important effects in the convergence of the solution.

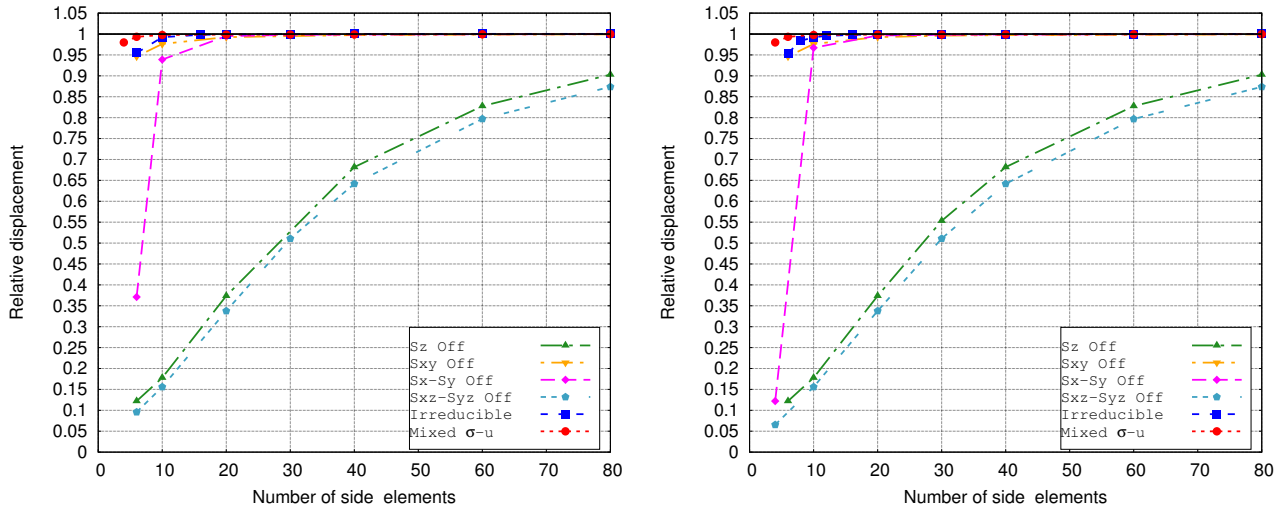

Figure 13: Scordelis-Lo roof: Stress deactivation convergence curves using $n_{\text{nelem}} = 2$ (left) and $n_l = 2$ (right).

6.2.2. Twisted beam

This problem was initially proposed in [83] to test the wrapping effect of elements. It consists in a cantilever twisted beam with a point load at the free end, which can be directed either in or out of the plane. The geometry and boundary conditions are illustrated in Fig. 14. The length of the beam is $L = 12$, the width is $W = 1.1$ and the twist is 90°. This test is usually performed using a moderate thickness of $t = 0.32$; however, in the present work it is set to $t = 0.0032$, which gives a slenderness ratio of $L/t = 3750$, to have even greater locking effects. The load

$P = 1$ is set outwards of the plane. As for the materials, Young's modulus is $E = 29 \cdot 10^6$ and Poisson's ratio is $\nu = 0.22$. The mesh is set using 8 elements along the width and increasing numbers of elements along the length. The solution is tracked at the center of the free end for the out-of-plane case, which has a horizontal displacement of 0.001294.

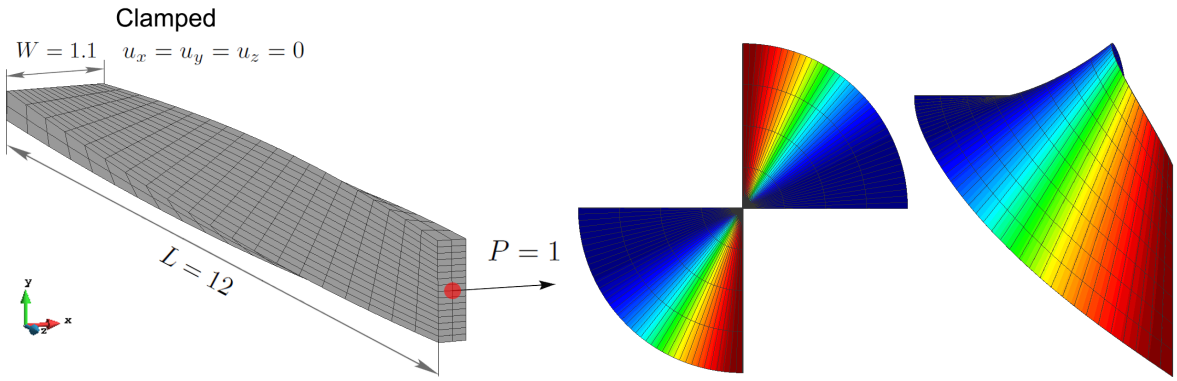

Figure 14: Twisted beam: geometry and boundary conditions (left) and deformed configuration (right).

Figure 15 shows the convergence curves of the relative displacement with respect to the number of elements using the irreducible and mixed formulations. Results show that the irreducible formulation can deal with numerical locking when computing using quadratic interpolation across the surface and through the thickness, but is affected by thickness locking when using linear interpolation in the transverse direction. Due to the small thickness of the shell, the locking effects are greatly amplified, as it occurs when using linear interpolations across the surface. On the other hand, the mixed formulation is free of shear, membrane and trapezoidal locking. Results clearly show that thickness locking can be overcome either by increasing the order of interpolation or the number of elements in the thickness direction.

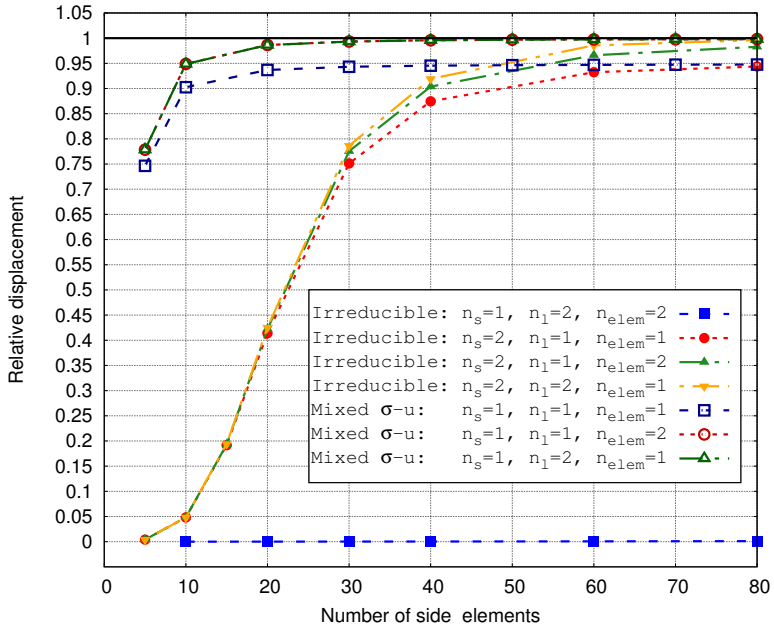

Figure 15: Twisted beam: convergence curves using irreducible and mixed formulations.

Even though both the twisted beam and Scordelis-Lo roof problems are membrane-dominated cases, they present different mechanical responses concerning stresses. When deactivating different stress groups, almost all stresses have to be interpolated to obtain proper convergence and avoid numerical locking, as shown in the convergence curves in Fig. 16. In this case, deactivating shear or twisting stresses yields locking of the solution. This is expected, considering that the problem undergoes strong shear locking effects due to the high slenderness ratio, even though

it is a membrane-dominated case. This problem also undergoes a high degree of element twisting, so it expected to need twisting stresses. Being a membrane-dominated case, it is natural that deactivating membrane stresses results in membrane locking. However, convergence curves show that membrane locking effects are much less severe compared with shear locking effects. In the case of trapezoidal locking, deactivating the thickness stress seems to have little impact on the solution, and convergence is similar to the irreducible formulation. On the other hand, thickness locking effects are mild; this becomes clear when comparing the solutions with $n_{\text{nelem}} = 2$ with $n_l = 2$, which are almost identical.

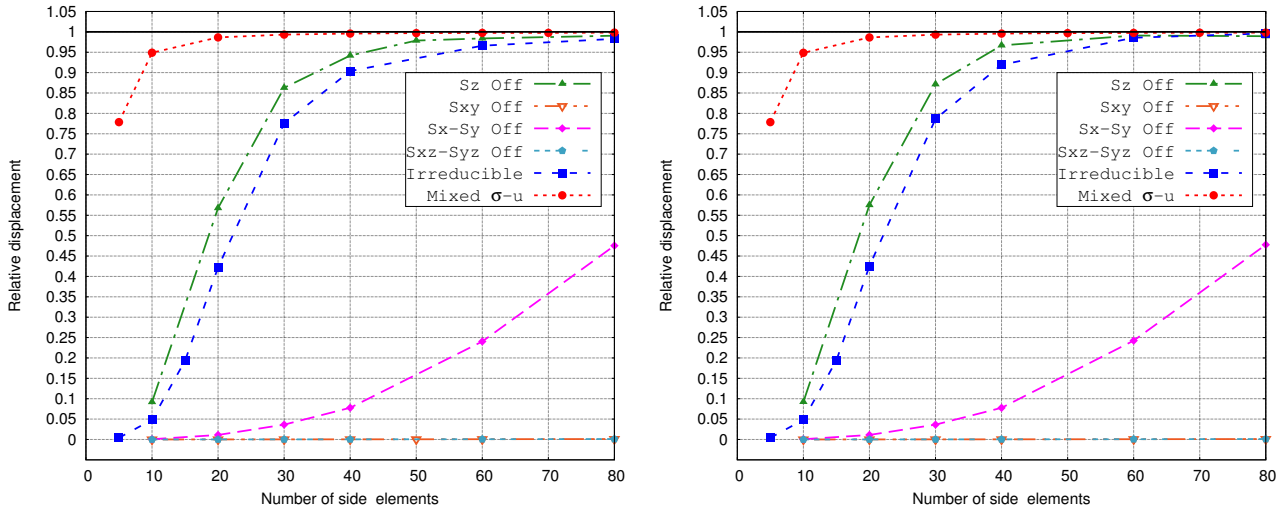

Figure 16: Twisted beam: Stress deactivation convergence curves using $n_{\text{nelem}} = 2$ (left) and $n_l = 2$ (right).

6.2.3. Hemispherical shell

This test is one step forward more challenging than the previous one because it tests both membrane and bending responses. It consists of a double curvature shell with a 18° hole, subject to point loads directed inwards and outwards of the surface. Due to the symmetry of the problem, only a quarter of the domain is modeled by using proper symmetry boundary conditions, as detailed in Fig. 17. The radius of the shell is $R = 10$, and the thickness is $t = 0.04$, which yields a slenderness ratio of $0.5R\pi/t = 392$. The loads are set to $P = 2$ each. The material properties are $E = 6.825 \cdot 10^7$ for Young's modulus and $\nu = 0.3$ for Poisson's ratio. Results are tracked at the points where forces are applied, where the normal displacements are 0.0940 according to the literature [83].

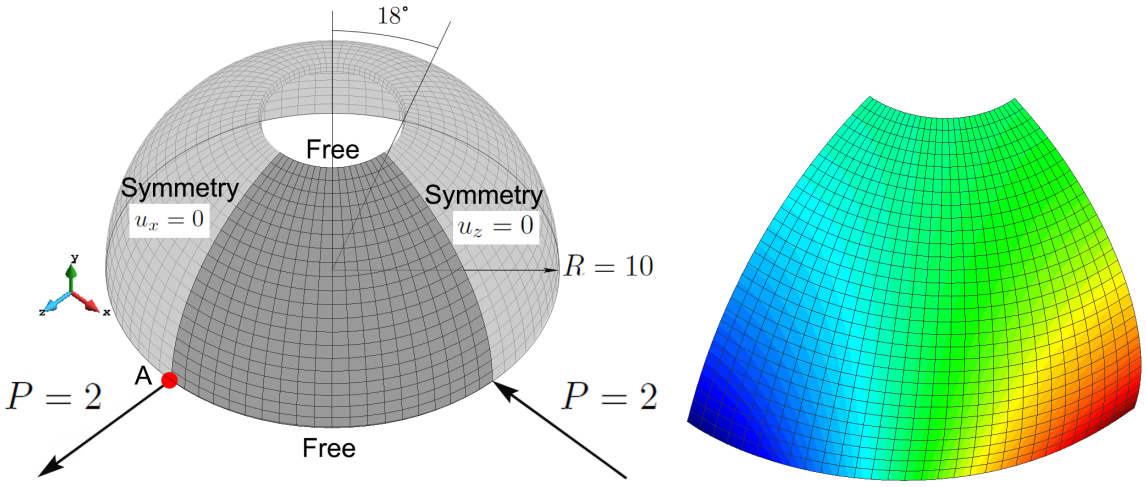

Figure 17: Hemispherical shell: geometry and boundary conditions (left) and deformed configuration (right).

Convergence curves for the irreducible and mixed formulations are shown in Fig. 18. Results show that thickness locking effects are almost negligible in all cases even though the Poisson ratio is relatively high. The stabilized mixed

and the irreducible quadratic formulations are free of numerical locking independently of the interpolation chosen in the thickness direction. It appears that even though the problem is mostly bending-dominated, locking conditions are not strong enough to need a richer interpolation through the thickness.

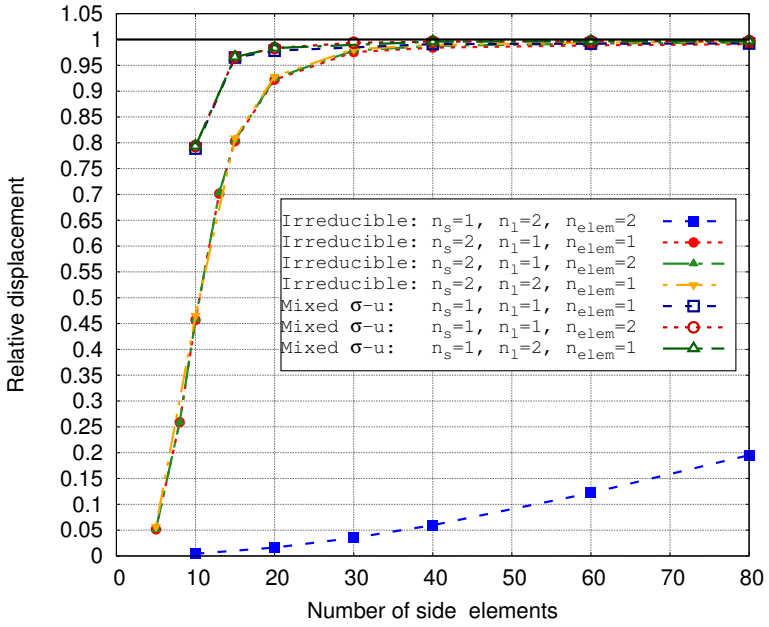

Figure 18: Hemispherical shell: convergence curves using irreducible and mixed formulations.

The convergence curves obtained when deactivating stress tensor components are plotted in Fig. 19. The curves behave in the same manner using either two elements or quadratic interpolation through the thickness. Results suggest that in this case trapezoidal locking is less relevant compared to shear and membrane locking, since the locking effect is milder when deactivating the thickness stress and stronger when deactivating the rest of the stresses. Even though the hemispherical shell problem is not designed to test element twisting, twisting stress appears to be necessary to capture the mechanical behavior of the shell.

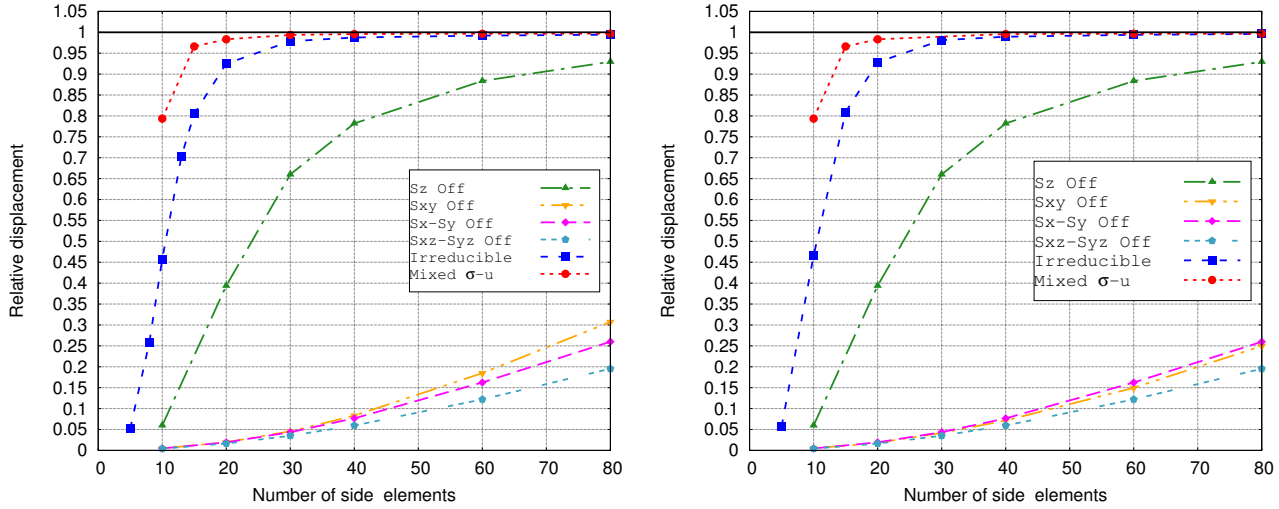

Figure 19: Hemispherical shell: Stress deactivation convergence curves using $n_{\text{nelem}} = 2$ (left) and $n_l = 2$ (right).

6.2.4. Pinched cylinder

This problem is the most demanding of the shell tests considered because it is subject to a high degree of inextensional bending. The test consists of a cylinder supported with one rigid diaphragm at each end, loaded

by two radial forces at the opposite sides of the middle of the length. Because of the symmetry of the problem, only the eighth part of the cylinder is modeled using proper symmetry boundary conditions. The geometry and boundary conditions are detailed in Fig. 20. The geometry of the cylinder is set using a length of $L = 600$, a radius of $R = 300$, and a thickness of $t = 3$. Therefore, the ratios of length and radius with respect to the thickness are $L/t = 200$ and $R/t = 100$, respectively. The material properties are $E = 3 \cdot 10^6$ for Young's modulus and $\nu = 0.3$ for Poisson's ratio. The loads are $P = 1$ each. The solution is tracked at the same point where the forces are applied, where the vertical displacement is $1.8384 \cdot 10^5$.

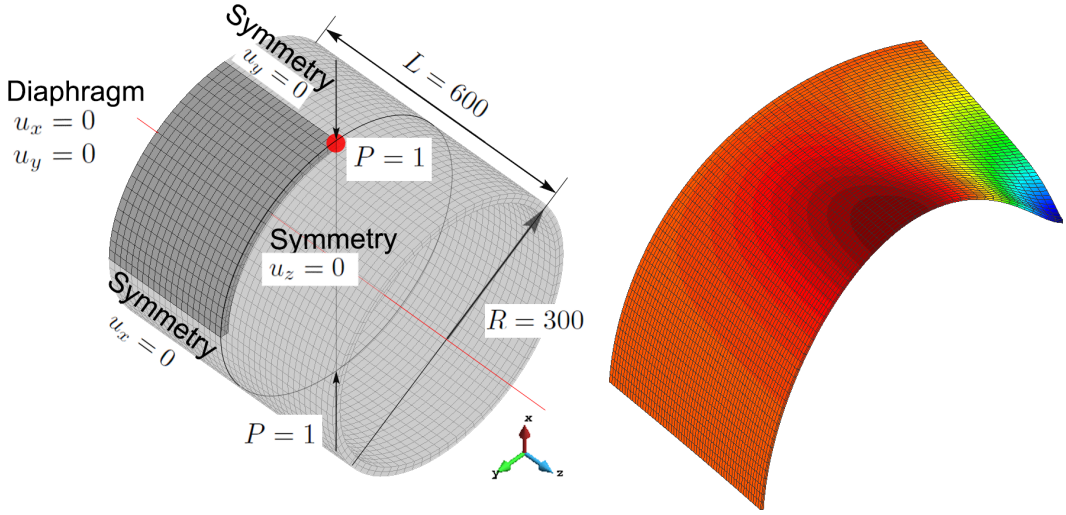

Figure 20: Pinched cylinder: geometry and boundary conditions (left) and deformed configuration (right).

The problem is solved for the irreducible and mixed formulations, whose convergence curves are plotted in Fig. 21. The thickness locking effects are stronger in this case compared with the rest of the tests. When using the irreducible formulation it becomes mandatory to use quadratic interpolation in the thickness direction, but with the mixed formulation this can also be overcome by using two elements in the thickness direction. With respect to the other types of locking, the mixed formulation is able to deal with them using only linear elements.

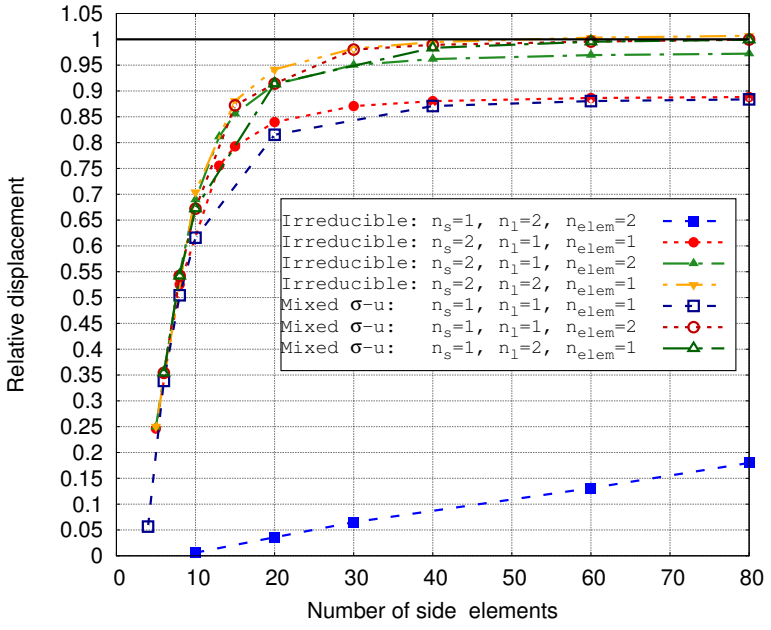

Figure 21: Pinched cylinder: convergence curves using irreducible and mixed formulations.

The convergence curves obtained by deactivating stress components are shown in Fig. 22. In this case, only the twisting stress can be turned off with no apparent locking effects. Results show that membrane, shear and

trapezoidal locking are of similar intensity since the curves obtained by neglecting the membrane, shear and thickness components of the stress, respectively, converge at a similar rate.

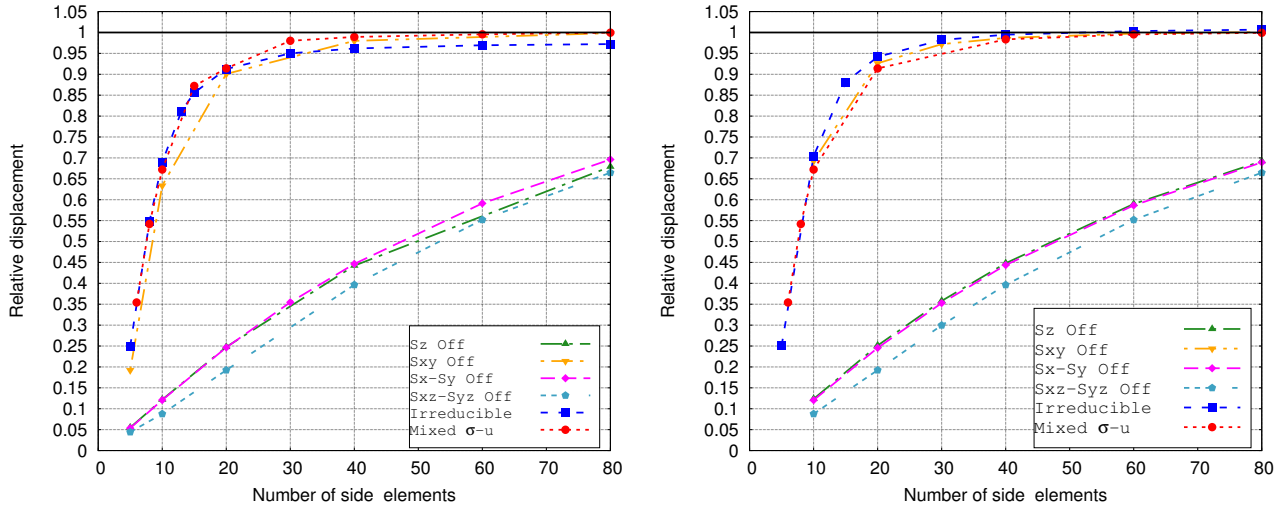

Figure 22: Pinched cylinder: Stress deactivation convergence curves using $n_{\text{nelem}} = 2$ (left) and $n_l = 2$ (right).

6.3. Result summary

The interpolation requirements and the mechanical response for plates and shells have been analyzed in subsections 6.1 and 6.2. Results show a variety of interpolation requirements to deal with numerical locking. In the irreducible formulation case, all tests have in common the need of using quadratic interpolation across the surface to deal with membrane, shear and trapezoidal locking, and quadratic interpolation in the thickness direction to deal with thickness locking. On the contrary, the mixed formulation allows to use linear elements in all directions, but it requires at least two elements in the thickness direction to deal with thickness locking. From the results it becomes clear that the bending-dominated problems are the most demanding cases in terms of interpolation, and some membrane-dominated problems can be solved using a single linear element in the thickness direction.

The stress requirements found for the mixed formulation in all numerical examples are summarized in Table 2. The type of locking and its intensity depend strongly on whether or not the structure is curved as well as on the bending state. Results are clear on the fact that shear locking is always present in thin structures, even in membrane-dominated states. From the results obtained, it becomes clear that curvature dramatically increases the complexity of thin structure problems. Moreover, this confirms that all stress components are required for a robust shell mixed formulation, since all of them are important in certain scenarios.

Case	Curvature	Mechanical response	Slenderness ratio	Membrane σ_x, σ_y	Twisting σ_{xy}	Thickness σ_z	Shear σ_{xz}, σ_{yz}
Circular plate	No	Bending	100	–	–	–	×
Square plate	No	Bending	200	–	–	–	×
Scordelis-Lo roof	Single	Membrane	200	–	–	×	×
Twisted beam	Double	Membrane	3750	×	×	–	×
Hemispherical shell	Double	Membrane >Bending	392	×	×	×	×
Pinched cylinder	Single	Bending >Membrane	200	×	–	×	×

Table 2: Stress tensor requirements for each benchmark test, required (×) and not-required (–).

7. Conclusions

The main purpose of this work is to study numerical locking in thin structures modeled by solid-shell elements using a mixed stabilized displacement-stress formulation. The study focuses on comprehending the locking mechanism by isolating the components of the stress field with respect to the local directors. To this end, the formulation is posed using curvilinear coordinates, and the components of the stress field can be grouped with respect to the direction they act: membrane, shear, twisting and thickness stresses. Additionally, an algorithm to independently activate or deactivate the components of the stress field has been implemented, allowing to solve numerical examples by interpolating only part of the stress tensor. A set of benchmark problems have been solved interpolating all the stress tensor and deactivating a single stress group at a time. Convergence curves have been plotted in order to characterize the mechanical response of the structure with respect to numerical locking. Results show which specific stress groups have to be interpolated in curved structures in order to circumvent numerical locking; these groups depend on the geometry, type of curvature, boundary conditions and type of load. Flat structures are easier to analyze: they suffer shear locking when subject to transverse loads, and they are also affected by thickness locking if the through-the-thickness interpolation is not rich enough to capture the behavior of the solution. As a result of the present investigation, it has been proven that a robust stabilized mixed formulation that can properly handle all types of mechanical behaviors of curved shells requires interpolating all the stresses and having either a minimum of two elements or quadratic interpolation through the thickness. Obviously, if all components of the stress tensor are interpolated, there is no need to use curvilinear coordinates.

Acknowledgement

This work was supported by Vicerrectoría de Investigación, Desarrollo e Innovación (VRIDEI) of the Univeridad de Santiago de Chile, and the National Agency for Research and Development (ANID) Doctorado Becas Chile/2019 - 72200128 of the Government of Chile. R. Codina acknowledges the support received from the ICREA Acadèmia Research Program of the Catalan Government.

References

[1] T. Belytschko, W. K. Liu, B. Moran, and K. Elkhodary, *Nonlinear finite elements for continua and structures*. John wiley & sons, 2014.

[2] E. Oñate, *Structural analysis with the finite element method. Linear statics: volume 2: beams, plates and shells*. Springer Science & Business Media, 2013.

[3] E. Reissner, "On one-dimensional finite-strain beam theory: the plane problem," *Zeitschrift für angewandte Mathematik und Physik ZAMP*, vol. 23, no. 5, pp. 795–804, 1972.

[4] R. H. Macneal, "Derivation of element stiffness matrices by assumed strain distributions," *Nuclear Engineering and Design*, vol. 70, no. 1, pp. 3–12, 1982.

[5] T. Belytschko and W. E. Bachrach, "Efficient implementation of quadrilaterals with high coarse-mesh accuracy," *Computer Methods in Applied Mechanics and Engineering*, vol. 54, no. 3, pp. 279–301, 1986.

[6] J. C. Simo, D. D. Fox, and M. S. Rifai, "On a stress resultant geometrically exact shell model. Part III: Computational aspects of the nonlinear theory," *Computer Methods in Applied Mechanics and Engineering*, vol. 79, no. 1, pp. 21–70, 1990.

[7] N. Büchter, E. Ramm, and D. Roehl, "Three-dimensional extension of non-linear shell formulation based on the enhanced assumed strain concept," *International Journal for Numerical Methods in Engineering*, vol. 37, no. 15, pp. 2551–2568, 1994.

[8] M. Bucalem and K.-J. Bathe, "Finite element analysis of shell structures," *Archives of Computational Methods in Engineering*, vol. 4, no. 1, pp. 3–61, 1997.

[9] M. Bischoff and E. Ramm, "Shear deformable shell elements for large strains and rotations," *International Journal for Numerical Methods in Engineering*, vol. 40, no. 23, pp. 4427–4449, 1997.

[10] I. Romero, "A comparison of finite elements for nonlinear beams: the absolute nodal coordinate and geometrically exact formulations," *Multibody System Dynamics*, vol. 20, no. 1, pp. 51–68, 2008.

[11] J. Valle, A. Albanesi, and V. Fachinotti, "An efficient general curvilinear coordinates finite element method for the linear dynamic study of thickness-independent shells," *Latin American Journal of Solids and Structures*, vol. 16, 2019.

[12] S. Ahmad, B. M. Irons, and O. Zienkiewicz, "Analysis of thick and thin shell structures by curved finite elements," *International Journal for Numerical Methods in Engineering*, vol. 2, no. 3, pp. 419–451, 1970.

[13] T. Kant, S. Kumar, and U. Singh, "Shell dynamics with three-dimensional degenerate finite elements," *Computers & structures*, vol. 50, no. 1, pp. 135–146, 1994.

[14] H. T. Yang, S. Saigal, A. Masud, and R. Kapania, "A survey of recent shell finite elements," *International Journal for Numerical Methods in Engineering*, vol. 47, no. 1-3, pp. 101–127, 2000.

[15] D. Marinković, H. Köppe, and U. Gabbert, "Degenerated shell element for geometrically nonlinear analysis of thin-walled piezoelectric active structures," *Smart Materials and Structures*, vol. 17, no. 1, p. 015030, 2008.

[16] P. Betsch, F. Gruttmann, and E. Stein, "A 4-node finite shell element for the implementation of general hyperelastic 3d-elasticity at finite strains," *Computer Methods in Applied Mechanics and Engineering*, vol. 130, no. 1-2, pp. 57–79, 1996.

[17] N. Buechter and E. Ramm, "Shell theory versus degeneration a comparison in large rotation finite element analysis," *International Journal for Numerical Methods in Engineering*, vol. 34, no. 1, pp. 39–59, 1992.

[18] N. Büchter and E. Ramm, "Comparison of shell theory and degeneration," in *Nonlinear Analysis of Shells by Finite Elements*, pp. 15–30, Springer, 1992.

[19] R. Hauptmann and K. Schweizerhof, "A systematic development of 'solid-shell' element formulations for linear and non-linear analyses employing only displacement degrees of freedom," *International Journal for Numerical Methods in Engineering*, vol. 42, no. 1, pp. 49–69, 1998.

[20] M. Bischoff, K.-U. Bletzinger, W. Wall, and E. Ramm, "Models and finite elements for thin-walled structures," *Encyclopedia of computational mechanics*, 2004.

[21] S. Doll, K. Schweizerhof, R. Hauptmann, and C. Freischläger, "On volumetric locking of low-order solid and solid-shell elements for finite elastoviscoplastic deformations and selective reduced integration," *Engineering Computations*, vol. 17, no. 7, pp. 874–902, 2000.

[22] K. Sze, "Three-dimensional continuum finite element models for plate/shell analysis," *Progress in Structural Engineering and Materials*, vol. 4, no. 4, pp. 400–407, 2002.

[23] R. H. MacNeal, "Toward a defect-free four-noded membrane element," *Finite elements in analysis and design*, vol. 5, no. 1, pp. 31–37, 1989.

[24] R. H. MacNeal, "A simple quadrilateral shell element," *Computers & Structures*, vol. 8, no. 2, pp. 175–183, 1978.

[25] K. Park and G. Stanley, "A curved C^0 shell element based on assumed natural-coordinate strains," *Journal of Applied Mechanics*, vol. 53, no. 2, pp. 278–290, 1986.

[26] J. Simo and Hughes, "On the variational foundations of assumed strain methods," *Journal of Applied Mechanics*, vol. 53, no. 1, pp. 51–54, 1986.

[27] J. C. Simo and M. Rifai, "A class of mixed assumed strain methods and the method of incompatible modes," *International Journal for Numerical Methods in Engineering*, vol. 29, no. 8, pp. 1595–1638, 1990.

[28] T. Belytschko and L. P. Bindeman, "Assumed strain stabilization of the eight node hexahedral element," *Computer Methods in Applied Mechanics and Engineering*, vol. 105, no. 2, pp. 225–260, 1993.

[29] S. Klinkel, F. Gruttmann, and W. Wagner, "A continuum based three-dimensional shell element for laminated structures," *Computers & Structures*, vol. 71, no. 1, pp. 43–62, 1999.

[30] K. Sze and L. Yao, "A hybrid stress ANS solid-shell element and its generalization for smart structure modelling. Part I: solid shell element formulation," *International Journal for Numerical Methods in Engineering*, vol. 48, no. 4, pp. 545–564, 2000.

[31] K. Sze, L. Yao, and S. Yi, "A hybrid stress ANS solid-shell element and its generalization for smart structure modelling. Part II: smart structure modelling," *International Journal for Numerical Methods in Engineering*, vol. 48, no. 4, pp. 565–582, 2000.

[32] K. Sze, S.-J. Zheng, and S. Lo, "A stabilized eighteen-node solid element for hyperelastic analysis of shells," *Finite Elements in Analysis and Design*, vol. 40, no. 3, pp. 319–340, 2004.

[33] K. Kim, G. Liu, and S. Han, "A resultant 8-node solid-shell element for geometrically nonlinear analysis," *Computational Mechanics*, vol. 35, pp. 315–331, 2005.

[34] A. Hajlaoui, M. Wali, M. B. Jdidia, and F. Dammak, "An improved enhanced solid shell element for static and buckling analysis of shell structures," *Mechanics & Industry*, vol. 17, no. 5, p. 510, 2016.

[35] M. Mostafa, M. Sivaselvan, and C. Felippa, "A solid-shell corotational element based on ANDES, ANS and EAS for geometrically nonlinear structural analysis," *International Journal for Numerical Methods in Engineering*, vol. 95, no. 2, pp. 145–180, 2013.

[36] J. Caseiro, R. F. Valente, A. Reali, J. Kiendl, F. Auricchio, and R. Alves de Sousa, "On the assumed natural strain method to alleviate locking in solid-shell NURBS-based finite elements," *Computational Mechanics*, vol. 53, pp. 1341–1353, 2014.

[37] J. Caseiro, R. Valente, A. Reali, J. Kiendl, F. Auricchio, and R. A. de Sousa, "Assumed natural strain NURBS-based solid-shell element for the analysis of large deformation elasto-plastic thin-shell structures," *Computer Methods in Applied Mechanics and Engineering*, vol. 284, pp. 861–880, 2015.

[38] J. Huang, S. Cen, Z. Li, and C.-F. Li, "An unsymmetric 8-node hexahedral solid-shell element with high distortion tolerance: linear formulations," *International Journal for Numerical Methods in Engineering*, vol. 116, no. 12-13, pp. 759–783, 2018.

[39] O. Zienkiewicz, R. Taylor, and J. Too, "Reduced integration technique in general analysis of plates and shells," *International Journal for Numerical Methods in Engineering*, vol. 3, no. 2, pp. 275–290, 1971.

[40] D. Naylor, "Stresses in nearly incompressible materials by finite elements with application to the calculation of excess pore pressures," *International Journal for Numerical Methods in Engineering*, vol. 8, no. 3, pp. 443–460, 1974.

[41] D. S. Malkus and T. J. Hughes, "Mixed finite element methods - reduced and selective integration techniques: a unification of concepts," *Computer Methods in Applied Mechanics and Engineering*, vol. 15, no. 1, pp. 63–81, 1978.

[42] T. Belytschko, J. S.-J. Ong, W. K. Liu, and J. M. Kennedy, "Hourglass control in linear and nonlinear problems," *Computer Methods in Applied Mechanics and Engineering*, vol. 43, no. 3, pp. 251–276, 1984.

[43] M. Schwarze and S. Reese, "A reduced integration solid-shell finite element based on the EAS and the ANS concept—Geometrically linear problems," *International Journal for Numerical Methods in Engineering*, vol. 80, no. 10, pp. 1322–1355, 2009.

[44] M. Schwarze and S. Reese, "A reduced integration solid-shell finite element based on the EAS and the ANS concept—Large deformation problems," *International Journal for Numerical Methods in Engineering*, vol. 85, no. 3, pp. 289–329, 2011.

[45] S. Reese, "A large deformation solid-shell concept based on reduced integration with hourglass stabilization," *International Journal for Numerical Methods in Engineering*, vol. 69, no. 8, pp. 1671–1716, 2007.

[46] M. Pagani, S. Reese, and U. Perego, "Computationally efficient explicit nonlinear analyses using reduced integration-based solid-shell finite elements," *Computer Methods in Applied Mechanics and Engineering*, vol. 268, pp. 141–159, 2014.

[47] L. Leonetti, F. Liguori, D. Magisano, and G. Garcea, "An efficient isogeometric solid-shell formulation for geometrically nonlinear analysis of elastic shells," *Computer Methods in Applied Mechanics and Engineering*, vol. 331, pp. 159–183, 2018.

[48] O. Barfusz, T. van der Velden, T. Brepols, H. Holthusen, and S. Reese, "A reduced integration-based solid-shell finite element formulation for gradient-extended damage," *Computer Methods in Applied Mechanics and Engineering*, vol. 382, p. 113884, 2021.

[49] K.-J. Bathe, *Finite element procedures*. Klaus-Jurgen Bathe, 2006.

[50] D. Chapelle and K.-J. Bathe, *The finite element analysis of shells-fundamentals*. Springer Science & Business Media, 2010.

[51] E. N. Dvorkin and K.-J. Bathe, "A continuum mechanics based four-node shell element for general non-linear analysis," *Engineering computations*, vol. 1, no. 1, pp. 77–88, 1984.

[52] K.-J. Bathe, A. Iosilevich, and D. Chapelle, "An evaluation of the MITC shell elements," *Computers & Structures*, vol. 75, no. 1, pp. 1–30, 2000.

[53] K.-J. Bathe, A. Iosilevich, and D. Chapelle, "An inf-sup test for shell finite elements," *Computers & Structures*, vol. 75, no. 5, pp. 439–456, 2000.

[54] H.-M. Jeon, Y. Lee, P.-S. Lee, and K.-J. Bathe, "The MITC3+ shell element in geometric nonlinear analysis," *Computers & Structures*, vol. 146, pp. 91–104, 2015.

[55] D. Chapelle, A. Ferent, and K. Bathe, "3d-shell elements and their underlying mathematical model," *Mathematical Models and Methods in Applied Sciences*, vol. 14, no. 01, pp. 105–142, 2004.

[56] T. Sussman and K.-J. Bathe, "3d-shell elements for structures in large strains," *Computers & structures*, vol. 122, pp. 2–12, 2013.

[57] M. Cinefra, "Formulation of 3d finite elements using curvilinear coordinates," *Mechanics of Advanced Materials and Structures*, vol. 29, no. 6, pp. 879–888, 2022.

[58] M. Rezaiee-Pajand and M. Ramezani, "An evaluation of MITC and ANS elements in the nonlinear analysis of shell structures," *Mechanics of Advanced Materials and Structures*, vol. 29, no. 26, pp. 4677–4697, 2022.

[59] T. J. Hughes, "Generalization of selective integration procedures to anisotropic and nonlinear media," *International Journal for Numerical Methods in Engineering*, vol. 15, no. 9, pp. 1413–1418, 1980.

[60] J. Simo, R. L. Taylor, and K. Pister, "Variational and projection methods for the volume constraint in finite deformation elasto-plasticity," *Computer methods in applied mechanics and engineering*, vol. 51, no. 1-3, pp. 177–208, 1985.

[61] K. Sze and A. Ghali, "Hybrid hexahedral element for solids, plates, shells and beams by selective scaling," *International Journal for Numerical Methods in Engineering*, vol. 36, no. 9, pp. 1519–1540, 1993.

[62] C. Sansour and F. Kollmann, "Families of 4-node and 9-node finite elements for a finite deformation shell theory. an assesment of hybrid stress, hybrid strain and enhanced strain elements," *Computational Mechanics*, vol. 24, pp. 435–447, 2000.

[63] Y. Kim and S. Lee, "A solid element formulation for large deflection analysis of composite shell structures," in *Computational Structural Mechanics & Fluid Dynamics*, pp. 269–274, Elsevier, 1988.

[64] H. C. Park, C. Cho, and S. W. Lee, "An efficient assumed strain element model with six dof per node for geometrically non-linear shells," *International Journal for Numerical Methods in Engineering*, vol. 38, no. 24, pp. 4101–4122, 1995.

[65] T. J. Hughes, "Multiscale phenomena: Green's functions, the Dirichlet-to-Neumann formulation, subgrid scale models, bubbles and the origins of stabilized methods," *Computer methods in applied mechanics and engineering*, vol. 127, no. 1-4, pp. 387–401, 1995.

[66] T. J. Hughes, G. R. Feijóo, L. Mazzei, and J.-B. Quincy, "The variational multiscale method—A paradigm for computational mechanics," *Computer methods in applied mechanics and engineering*, vol. 166, no. 1-2, pp. 3–24, 1998.

[67] R. Codina, "Stabilization of incompressibility and convection through orthogonal sub-scales in finite element methods," *Computer methods in applied mechanics and engineering*, vol. 190, no. 13-14, pp. 1579–1599, 2000.

[68] R. Codina, "Stabilized finite element approximation of transient incompressible flows using orthogonal subscales," *Computer methods in applied mechanics and engineering*, vol. 191, no. 39-40, pp. 4295–4321, 2002.

[69] E. Castillo and R. Codina, "Finite element approximation of the viscoelastic flow problem: A non-residual based stabilized formulation," *Computers & Fluids*, vol. 142, pp. 72–78, 2017.

[70] L. Moreno, R. Codina, J. Baiges, and E. Castillo, "Logarithmic conformation reformulation in viscoelastic flow problems approximated by a VMS-type stabilized finite element formulation," *Computer Methods in Applied Mechanics and Engineering*, vol. 354, pp. 706–731, 2019.

[71] I. Castañar, R. Codina, and J. Baiges, "A stabilized mixed three-field formulation for stress accurate analysis including the incompressible limit in finite strain solid dynamics," *International Journal for Numerical Methods in Engineering*, vol. 124, no. 10, pp. 2341–2366, 2023.

[72] A. Fabra and R. Codina, "Mixed stabilized finite element methods in linear elasticity for the velocity–stress equations in the time and the frequency domains," *Computer Methods in Applied Mechanics and Engineering*, vol. 404, p. 115777, 2023.

[73] R. Codina, "Finite element approximation of the three-field formulation of the Stokes problem using arbitrary interpolations," *SIAM Journal on Numerical Analysis*, vol. 47, no. 1, pp. 699–718, 2009.

[74] K. Washizu, "Variational methods in elasticity and plasticity," *International Series of Monographs in Aeronautics and Astronautics*, 1968.

[75] D. Boffi, F. Brezzi, and M. Fortin, *Mixed Finite Element Methods and Applications*. Springer, 2013.

[76] M. Cervera, M. Chiumenti, and R. Codina, "Mixed stabilized finite element methods in nonlinear solid mechanics: Part i: Formulation," *Computer Methods in Applied Mechanics and Engineering*, vol. 199, no. 37-40, pp. 2559–2570, 2010.

[77] S. Saloustros, M. Cervera, S. Kim, and M. Chiumenti, "Accurate and locking-free analysis of beams, plates and shells using solid elements," *Computational Mechanics*, vol. 67, no. 3, pp. 883–914, 2021.

[78] R. Codina, J. Principe, and J. Baiges, "Subscales on the element boundaries in the variational two-scale finite element method," *Computer Methods in Applied Mechanics and Engineering*, vol. 198, no. 5-8, pp. 838–852, 2009.

[79] R. Codina, S. Badia, J. Baiges, and J. Principe, "Variational multiscale methods in computational fluid dynamics," *Encyclopedia of Computational Mechanics, Second Edition*, pp. 1–28, 2018.

[80] R. Hauptmann, K. Schweizerhof, and S. Doll, "Extension of the 'solid-shell' concept for application to large elastic and large elastoplastic deformations," *International Journal for Numerical Methods in Engineering*, vol. 49, no. 9, pp. 1121–1141, 2000.

[81] H. Zhang and J. S. Kuang, "Eight-node Reissner–Mindlin plate element based on boundary interpolation using Timoshenko beam function," *International Journal for Numerical Methods in Engineering*, vol. 69, no. 7, pp. 1345–1373, 2007.

[82] A. Aguirre, R. Codina, and J. Baiges, "A variational multiscale stabilized finite element formulation for Reissner–Mindlin plates and Timoshenko beams," *Finite Elements in Analysis and Design*, vol. 217, p. 103908, 2023.

[83] R. H. Macneal and R. L. Harder, "A proposed standard set of problems to test finite element accuracy," *Finite elements in analysis and design*, vol. 1, no. 1, pp. 3–20, 1985.

[84] T. Belytschko, H. Stolarski, W. K. Liu, N. Carpenter, and J. S. Ong, "Stress projection for membrane and shear locking in shell finite elements," *Computer Methods in Applied Mechanics and Engineering*, vol. 51, no. 1-3, pp. 221–258, 1985.

[85] J. C. Simo and D. D. Fox, "On a stress resultant geometrically exact shell model. Part I: Formulation and optimal parametrization," *Computer Methods in Applied Mechanics and Engineering*, vol. 72, no. 3, pp. 267–304, 1989.

[86] T. Belytschko, B. L. Wong, and H. Stolarski, "Assumed strain stabilization procedure for the 9-node Lagrange shell element," *International Journal for Numerical Methods in Engineering*, vol. 28, no. 2, pp. 385–414, 1989.